Electrokinetic evaluation of human articular cartilage

by

John W. Lin

Submitted to the Department of Electrical Engineering and Computer Science
in partial fulfillment of the requirements for the degree of

Master of Engineering in Electrical Engineering and Computer Science

at the

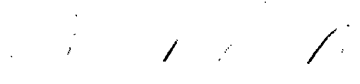MASSACHUSETTS INSTITUTE OF TECHNOLOGY

September 1995

Author . . . .
Department of Electrical Engineering and Computer Science
June 23rd, 1995
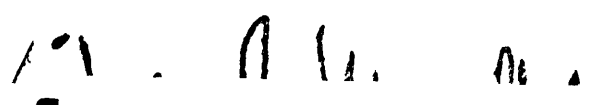
Certified by . . . .
Alan J. Grodzinsky
Professor of Electrical, Mechanical, and Bioengineering
Thesis Supervisor

Accepted by . . . .
Frederic R. Morgenthaler
Chairman, Department Committee on Graduate Theses

Electrokinetic evaluation of human articular cartilage

by

John W. Lin

Abstract

This thesis describes the *in vitro* testing of human acetabular cartilage from an 82-year old male patient who had an instrumented femoral endoprosthesis implanted in his left hip. The dynamic mechanical and streaming potential responses of cartilage from nine locations in the left and right acetabula are measured in uniaxial confined compression, with the tissue hydration and glycosaminoglycan content subsequently assayed. Results indicate no significant variation between the left and right acetabula of the patient, although mechanical properties varied significantly by location within each acetabulum. Striking differences in the electromechanical properties of the superficial and deep zones suggest inhomogeneity in the tissue. In the deep zone, the mean hydraulic permeability (k_p) was $2.36 \times 10^{-15} m^2/Pa\ sec$, and the mean electrokinetic coefficient (k_e) was $1.87 \times 10^{-9} V/Pa$. The mean equilibrium modulus (H_A) of all cartilage samples was $368 kPa$. Trends in tissue hydration versus GAG content suggest potential damage to the tissue's collagen or matrix network. Streaming potential amplitude correlated strongly with equilibrium modulus and GAG content (as % of dry weight), consistent with previous studies of electrokinetics in degraded bovine and rabbit knee cartilage.

Acknowledgments

Contrary to what's written on the title page, this thesis is the product of many people's labors, and I would like to thank them all for their kind efforts.

Fellow students at M.I.T. have described Professor Alan J. Grodzinsky as a divine entity in academia, on account of his teaching skill and personability. His support, advice, criticisms, and encouragement have sustained the research reported in this thesis, but his simply being a nice guy has sustained his entire lab. The energy and sheer happiness of his students are palpable! The pleasure of working in Al's environment has changed my perception of research, and redefined my vision of a successful lab.

I am also indebted to Dr. Chris McGibbon and Dr. David E. Krebs for their interest in electromechanical evaluation of the acetabula from the instrumented endoprothesis study. Literally, this thesis would not have been possible without them. I am especially grateful to Chris McGibbon for his assistance and consultation throughout the study. Dr. Stephen B. Trippel graciously contributed his expertise and volunteered his time to perform histological studies of the acetabular cartilage. His histological assessments will be of great importance in interpreting the data collected in this study. It was an honor and pleasure to work with them.

The contributions of Dr. Eliot Frank, lab guru, are omnipresent in the lab. He has rescued me on several occasions when I ran afoul. I recall with a smile the first time I tried, in vain, to use the DynaStat; Eliot dropped what he was doing, took a look at what I was doing, and showed me the "ON" switch to the power amplifier. He greatly assisted me throughout the experiments described in this thesis, and his parameter estimation code made data analysis almost too easy.

"Probe"rs Scott Berkenblit, Dave Bombard, and Steve Treppo have been a continuing source of wisdom, advice, and humor. As both Steve and I jumped on board Al's ship at about the same time, his perspective and his comments have been great sources of guidance. Scott, the senior Prober, is either crazy or saintly for still helping out novices like me while he's slaving away during medical school rotations. Dave was always there at the front lines of combat working on the hand-held probe, and demonstrated many times that he was the master of practical problem solving. Moreover, like Al, Dave's energy and personality were positively infectious, making the working day not much like work at all.

Jane Murray, lab guru-ess, showed me the ropes around the lab and taught me how to do the biochemical assays used herein. Even though I would ask the same question three times in three months, she was always happy to help. Minerva Garcia (a Ph.D. candidate) is also a consummate teacher and scientist, often taking the initiative to offer advice or assistance. She, along with Jennifer Stinn, are like magicians in making cartilage explantation look so easy.

Finally, I would like to acknowledge the personal contributions of Julia Su. Thank you for always being there, and thank you for your laughter. I shall always remember these days fondly.

Contents

Chapter 1

Introduction

Articular cartilage, an unmineralized tissue, is remarkably capable of withstanding the high-load conditions of the articular joint. The same factors that enable cartilage to endure such compressive stresses also give rise to an electromechanical coupling within cartilage itself. Previous studies of articular cartilage have shown that we can observe this coupling by applying a fixed mechanical displacement to cartilage and measuring the resultant electrical response; further, this electrokinetic coupling strongly correlates with the presence of a fixed charge density within the tissue. Such experiments have been conducted with bovine tissue taken from the femoropatellar groove and with cartilage from rabbit and guinea pig knee joints. In anticipation of the clinical applications of such results, this thesis focuses on electrokinetic studies with human articular cartilage, and compares the behavior of human and bovine tissue.

1.1   Cartilage extracellular matrix

Cartilage is, in comparison with other soft connective tissues, sparsely populated with cells (10% by volume) [34]. Cartilage tissue is highly hydrated, being composed of 60% − 80% fluid by weight. The actual extent of hydration is a function of both the proteoglycan-associated swelling pressures and the restoring tension of the collagen network [25]. The majority of the tissue volume is occupied by a complex, hydrated extracellular matrix (ECM) [7].

5

The compressive stiffness of articular cartilage is intimately related to this ECM, which is composed of collagens, predominantly type II, and various proteoglycans, including aggrecan. Collagen contributes roughly 50% of the tissue dry weight [8]. These collagen fibrils form a network whose primary mechanical function is tension, especially in resistance to the cartilage's tendency to swell or stretch [25]. There are several types of collagen present in cartilage, and biochemical analyses reveal several sites for intra- and inter-fibril cross-linking [12]. Type IX collagen, present in small amounts (1%) in adult cartilage, is unique in having a glycosaminoglycan molecule associated with the molecule itself [8] as well as cross-linking sites to the bulk type II collagen fibrils. Thus, type IX collagen has been implicated in interactions with the proteoglycan matrix.

Proteoglycans have been described in numerous reviews [20, 31, 34] and are important in the normal mechanical function of cartilage. They are generally accepted as the origin of the swelling pressure in cartilage, and contribute the primary resistance to compressive loads [19]. Proteoglycans are large polysaccharide–protein macromolecules; aggrecan, the most common proteoglycan, is often pictured with a "wire-brush"-like structure. Each proteoglycan unit consists of a single core protein and one or more glycosaminoglycan (GAG) chains that extend radially from the core protein. For example, aggrecan, the most common proteoglycan in articular cartilage, consists of a 210 kDa protein core with over 100 GAGs covalently bonded to serine and threonine residues on the core protein. Moreover, many aggrecan molecules can be bound to a single hyaluronic acid chain stabilized by link protein, to form a proteoglycan aggregate which is more easily retained wihtin the matrix.

Individual GAG chains are long polymers of disaccharides. Chondroitin sulfate is the predominant of the two GAG types associated with aggrecan, and consists of glucuronic acid-N-acetylgalactosamine repeats [34]. At physiologic pH, there are two charge groups per repeated disaccharide: one from the ionized carboxylate on glucuronic acid, and another from the sulfate group bound to the N-acetylgalactosamine.

1.2 Electrokinetics

The negative fixed charge density of the ECM generates a local electric field around the GAG chains. This field is counterbalanced by an aggregation of positive counter-ions and concomitant exclusion of negative co-ions, consistent with a Poisson-Boltzmann distribution of the aqueous ions. The close proximity of proteoglycan GAG chains, with spacings on the order of a Debye length, results in a net repulsive interaction between the double layer fields associated with the GAG chains. The spacing decreases further during compression, thereby causing an increased repulsive force. Thus despite its hydrated nature, cartilage maintains a significant equilibrium compressive modulus [19].

In addition to this static resistance to compression, this conceptual model of ECM structure also predicts a dynamic transduction between electrical and mechanical forces. Since the fluid near the GAG chains has a net positive charge (excess counter-ions and excluded co-ions), a bulk flow of fluid results in the convective displacement of electrical charge. Displacement of charge produces an electric potential difference, and this differential potential is termed the streaming potential. Conversely, an applied electrical current will drive the mobile ions and generate a net fluid flow [18].

It has been demonstrated that uniaxial confined compression of cartilage between an impermeable substrate and a porous platen will produce measurable streaming potentials [15]. In addition, it has been demonstrated that applying a current to the surface of a cartilage disk will produce a detectable stress at the surface [3]. Furthermore, analytical models [16, 32] based on linear electrokinetic theory have been developed, and these models seem to predict the data previously observed during one-dimensional confined compression of bovine articular cartilage.

The model developed by Frank and Grodzinsky (1987b) applies for small input strains, where tissue behavior obeys the linearized phenomenological relation

$$
\begin{bmatrix} \vec{U} \\ \vec{J} \end{bmatrix} = \begin{bmatrix} -k_{11} & k_{12} \\ k_{21} & -k_{22} \end{bmatrix} \begin{bmatrix} \nabla P \\ \nabla V \end{bmatrix}
\tag{1.1}
$$

In this relation $\vec{U}$ is the area-averaged fluid velocity relative to the solid matrix, $\vec{J}$ is the

7

electric current density, ∇P is the gradient in hydraulic pressure, and ∇V is the gradient in electric potential. The diagonal coeffecients k_{11} and k_{22} are simply the "short-circuit" hydraulic permeability and the "no-flow" electric conductivity of the medium. The cross-coeffecients k_{12} and k_{21} embody the electromechanical transduction and will modify the observed hydraulic permeability in the presence of a voltage gradient. In an electrically open circuit ($\vec{J} = 0$), the electromechanical coupling results in the following expression for the Darcy hydraulic permeability:

$$k_p \equiv \frac{\vec{U}}{-\nabla P} = k_{11} - \frac{k_{12}k_{21}}{k_{22}}$$

During uniaxial confined compression, the complex exponential transfer function between an applied sinusoidal, compressive strain and the observed sinusoidal stress is given by

$$\frac{\sigma_{dyn}}{u_o/\delta} = \frac{K_s H_A \gamma \delta \coth \gamma \delta}{K_s + H_A \gamma \delta \coth \gamma \delta} \tag{1.2}$$

where σ_{dyn} is the dynamic stress amplitude, u_o is the applied dynamic displacement amplitude, δ is the plug thickness, K_s is the series stiffness of the porous platen (assumed to be lossless), and H_A is the equilibrum modulus. The reciprocal of γ is a skin depth-like length constant; its frequency dependence is evident in its definition

$$\gamma = \sqrt{\frac{j\omega}{H_A k_p}}$$

where k_p is the open-circuit hydraulic permeability as defined above.

Furthermore, the model predicts that the streaming potential amplitude is given by the equation

$$\frac{V_{str}}{u_o/\delta} = k_e \left[\frac{K_s H_A \gamma \delta \tanh \frac{\gamma \delta}{2}}{K_s + H_A \gamma \delta \coth \gamma \delta} \right] \tag{1.3}$$

The electrokinetic coupling coefficient k_e in terms of the k_{ij} of equation 1.1 is

$$k_e = \frac{k_{21}}{k_{22}}$$

This model predicts that the mechanical parameters K_s, H_A and k_p alone completely

determine the frequency dependence and phase of the streaming potential as well as the dynamic stiffness. Given equations 1.2 and 1.3, it is then possible to estimate the material parameters H_A, k_p, and k_e from experimental measurements of dynamic stress and streaming potential.

1.3 Osteoarthritis

Osteoarthritis is a common disease of articular joints, affecting a significant number of Americans 45 years of age or older [14, 28]. Afflicted tissue is deficient in proteoglycans [33], as well as more hydrated [24]. Damage to the collagen network has been implicated in this increased hydration. The mechanical properties of osteoarthritic cartilage are also compromised, as the compressive modulus decreases [30].

In the diagnosis of osteoarthritis, the two primary tools are radiography and arthroscopic visual assessment [14, 28]. The presence of a narrowed joint space and osteophytes on a radiograph, or arthroscopic visualization of cartilage fibrillation are both indicative of advanced osteoarthritis.

Unfortunately, such techniques may not be suited to the early detection of osteoarthritis. Histological and biochemical analyses of osteoarthritic cartilage show a marked alteration of ECM, particularly the loss of GAGs, during the early stages of osteoarthritis. This loss occurs first in the articular surface of the cartilage, and extends deeper towards the subchondral bone as the disease progresses [4]. Thus, in the early stages, there is ECM alteration and subsequent alterations of mechanical resiliency without visible or radiologic symptoms.

1.4 Clinical applications of electrokinetics

Notably, the electrokinetic behavior of articular cartilage is highly sensitive to the proteoglycan content within the ECM. Thus one would reasonably expect that observations of electrokinetic phenomena will be a more sensitive index of cartilage degradation than visual or radiographic assessment. Such clinical applications provide strong motivation for

the clarification of cartilage electrokinetic phenomena and development of tools for easily obtaining such information.

Electromechanical behavior of cartilage is elicited by applying an electrical or mechanical driving force and then observing the resultant mechanical or electrical response. Two principal experimental protocols are uniaxial confined compression [15] and current-driven surface spectroscopy [3]. These measurement protocols have been successfully applied on adult bovine tissue obtained from the femoropatellar groove. In contrast to the benchtop, *in vitro* nature of these previous experiments, recent work has produced a portable device and protocol that may ultimately be feasible for arthroscopic procedures [5].

The clinical application of such technology depends upon two prerequisites. First, the measurement technology must be practical to use *in vivo*; the recent work on scaling probe technology for hand-held, arthroscopic applications promotes this technology as a minimally invasive procedure. Second, we must understand the behavior of human cartilage and catalog measurements from normal and pathological subjects. This thesis addresses this second issue, in which the confined compression methodology is applied to cartilage from human acetabula.

Chapter 2

Background and Methods

The human acetabular cartilage used in this study was obtained from an 82-year old male, as part of a larger experimental study [23]. In December 1991 this patient underwent hemi-arthroplasty for a fracture in his left femoral neck, and consented to the implantation of a special endoprosthesis that was instrumented with pressure and temperature sensors underneath the surface. This prosthesis was largely similar in construction to the endoprosthesis used previously in a 73-year old female [22, 9], with changes in the spatial distribution of pressure sensors, the addition of a temperature sensor, and improvements in the telemetry system. The mechanical design of the two prostheses were largely identical. Using this implanted prosthesis, the investigators were able to monitor *in vivo* pressure distributions in the patient's joint over the course of several years.

Radiographs and visual observations during surgery did not indicate any extant joint degenerative disease. The patient died in October 1994 of renal kidney failure, after which the original investigators removed the implanted femoral head and harvested the corresponding acetabulum. As a control, the investigators also harvested the acetabulum of the right hip.

The electromechanical testing of this acetabular cartilage comes after mechanical testing of the intact acetabula with the prosthesis, as well as MRI imaging of the acetabula themselves. After electromechanical testing, several interesting sections of articular cartilage and several osteocartilaginous blocks were prepared for future histological examination. In the larger view, all of these results will be considered together in order to characterize the

physical properties of these human joint specimens.

2.1 Sample preparation

The acetabula were previously mounted in poly-methyl methacrylate (PMMA) to facilitate mechanical testing and MRI imaging. Following those tests the acetabula were stored at -70^oC until ready for electromechanical testing. Cylindrical cores $9.5mm$ in diameter and 1 to $3cm$ long were drilled from the acetabula using methods described previously [15]. Seven cores were taken from the left acetabulum, and six cores were taken from the right acetabulum, as illustrated in Figure 2-1. Cores 1 through 6 were taken on a 45° elevation from the anterior to superior to posterior axes; core 7 was taken on the superior axis lateral to core 4, at a 60° elevation.

For future comparisons against the MRI images of the acetabula, the thickness of the cartilage on these cores was determined by photographing transverse views of the core in each of four rotations about its cylindrical axis; distances on the photographs were calibrated against a slide with a $2mm$ long micrometer marked in $10\mu m$ divisions. These observed distances are indicated in Figure 2-1. The cores were then frozen at -20^oC until ready for experimentation.

In preparation for electromechanical testing, each core was thawed in a solution of $0.10M$ phosphate buffered saline with protease inhibitors ($0.01M$ EDTA, $1.0\mu M$ pepstatin, $1mM$ PMSF, phenylmethylsulfonylfluoride); after thawing, the core was mounted in a microtome. Between $25\mu m$ to $100\mu m$ of the superficial cartilage was removed to achieve a planar surface. A $9.5mm$ diameter full-thickness disk of cartilage was then sectioned and stored in the bath solution; the disk thickness so obtained varied between $500\mu m$ and $1mm$. Several cores along the anterior and posterior axis (cores 1 and 6 from the left hip, and core 6 from the right hip) were discarded, since the articular surface was primarily non-cartilaginous soft tissue. Core 3 on the right hip was also unusable since the microtoming resected subchondral bone along with the articular cartilage.
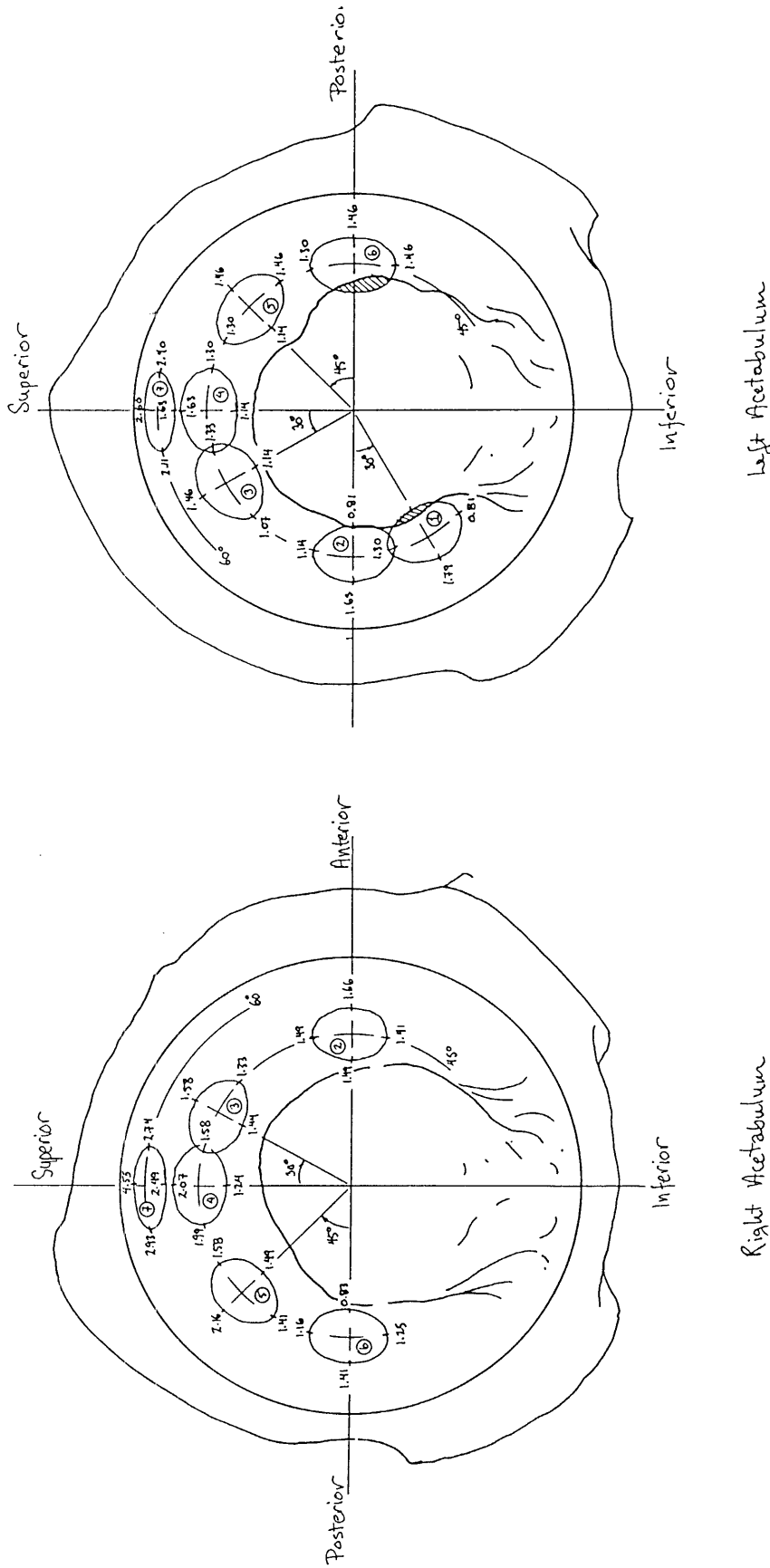
Figure 2-1: Hand-drawn representation and numbering of the core locations in both left and right acetabula. The four numbers about each core indicate the observed thickness (in *mm*) of the cartilage at the corresponding location. Cylindrical cores appear as ellipses due to the projection onto a 2-D plane. (Drawn by Dr. Chris McGibbon)

2.2 Electromechanical testing

The cartilage disk was then punched to form a smaller $6.35mm$ diameter circular plug and a surrounding annular ring. The plug's thickness was measured with a micrometer (see Appendix Table A.1). The plug was then placed in an electrically insulating testing chamber filled with the bath solution, as previously described for streaming potential measurements under uniaxial confined compression [15]. The chamber itself was mounted in a DynaStat mechanical spectrometer (IMASS, Hingham, MA). The lower surface of the cartilage plug was in direct contact with a $6.35mm$ diameter Ag/AgCl electrode (Annex Research, Costa Mesa, CA). The upper surface was in direct contact with a porous polyethylene platen; the platen itself was then compressed by the upper jaw of the DynaStat device. A second Ag/AgCl pellet electrode in the bath allowed for a differential potential measurement across the cartilage plug. The high input-impedance of the streaming potential pre-amplifier allows us to neglect Ohmic or capacitive losses in the hydrated platen and saline bath. Figure 2-2 schematically depicts the experimental setup.

Electromechanical testing involved the application of a static compressive strain to the cartilage plug. The tissue was allowed to equilibrate after the application of the strain. The mechanical stimulus consisted of a 1% sinusoidal strain superimposed on the static offset, at several frequencies between $1Hz$ and $0.002Hz$. The displacement and load outputs of the DynaStat, and the differential potential across the cartilage plug were low-pass filtered at $15.7Hz$ and recorded on a computer. At each frequency the static load, dynamic load, and streaming potential drop across the cartilage plug were averaged over two cycles of stimulation and then Fourier decomposed to give the response at that stimulus frequency. The total harmonic distortion (THD) of the dynamic load and the streaming potential was also recorded, serving as an indicator of output linearity (THD $\equiv \sqrt{\sum x_i^2}$, where x_i is the fractional content of the i'th harmonic).

The plugs were initially loaded with the articular surface contacting the porous platen. Electromechanical measurements were made at static offsets of 14%, 16%, and 15% (in that order); the tissue was allowed to equilibrate between each static offset. Then the cartilage plug was removed and loaded with the opposite surface (i.e., the deep cartilage)

to load cell

porous
platen

cartilage

chamber

V_{str}

$-$

$+$

Ag/AgCl
electrodes

to actuator
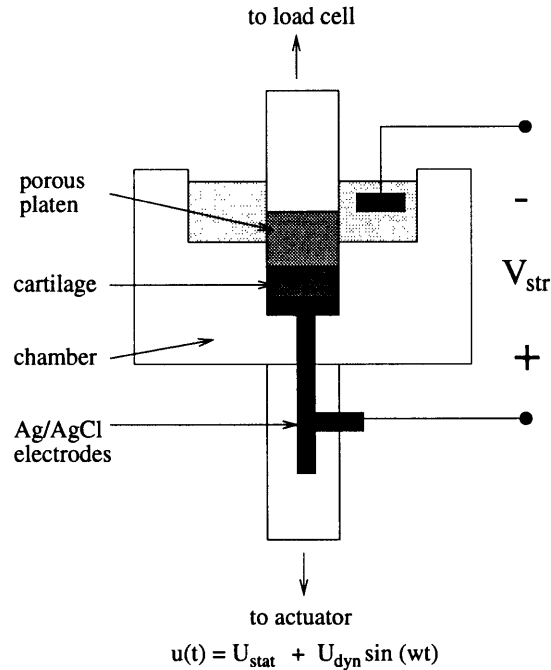
$u(t) = U_{stat} + U_{dyn} \sin(wt)$

Figure 2-2: Schematic diagram of the uniaxial confined compression streaming potential experiment. A sinusoidal displacement is applied at the actuator, and the resultant stress is measured at the load cell. The differential potential across the cartilage is measured through two Ag/AgCl pellet electrodes, one contacting the cartilage and one suspended in the bath. The actuator is oriented so that a compressive strain corresponds to a decreasing $u(t)$, hence the polarity of the V_{str} electrodes. A porous polyethylene platen on the upper surface of the cartilage provides a porous boundary condition on that surface.

contacting the porous platen. Measurements were again made, but only at a static offset of 15%. Plug 7 from the left acetabulum was not measured with the deep cartilage facing the platen due to substantial baseline drift in the electrical measurements. Plug 4 from the right acetabulum was not recorded at $0.01 Hz$ due to substantial noise in the measurements at low frequencies.

The non-linear least squares Levenberg-Marquardt algorithm was used to estimate material parameters from the mechanical and electromechanical data, as predicted by the model equations 1.2 and 1.3 [16]. The equation for the dynamic stiffness was used to fit three parameters: platen stiffness K_s, equilibrium modulus H_A, and open-circuit hydraulic permeability k_p. Given these three parameters, the best-fit k_e was then determined from the streaming potential data.

2.3 Biochemical analysis

After experimentation the plugs were removed from the bath, dabbed carefully to remove surface water, and then weighed to determine the cartilage's wet (hydrated) weight. The disk was then lyophilized overnight and re-weighed to determine the tissue dry weight.

The tissue was then digested in a solution of phosphate buffered EDTA ($0.10M$ sodium phosphate, $0.01M$ EDTA, pH 6.5) and 5 units/mL of protease K (a serine protease, Boehringer Mannheim). After 24 hours another 4 units/mL of protease K was added to ensure complete digestion. The sulfated GAG content of the plugs was then measured by aliquotting $15\mu l$ of the digests into $3ml$ of dimethylmethylene blue dye (DMMB, VWR, Boston, MA) and measuring the absorbance at $525nm$ [13]. The absorbance data was calibrated using known standards of shark chrondroitin-6-sulfate (Sigma).

Chapter 3

Results

This chapter will highlight significant trends and observations from the data. For reference, the Appendix compiles a more exhaustive series of scatter plots of mechanical and electromechanical parameters against the cartilage hydration and GAG content, as well as the relation between the observed streaming potential and several other functionally important cartilage parameters.

3.1 Cartilage orientation

A striking difference was observed in mechanical and electromechanical behavior depending upon cartilage orientation. Figure 3-1 shows that much larger streaming potentials were observed when the deep cartilage was in contact with the porous platen ("deep-oriented") than when the articular surface of the plug was in contact with the porous platen ("surface-oriented"). The streaming potential in many of the surface-oriented plugs did not monotonically decrease with decreasing frequency. In several surface-oriented plugs (L4, R4, R5) the streaming potential amplitude was actually larger at $0.01Hz$ than at $1.0Hz$. In contrast, in the deep-orientation the streaming potentials (with the exception of R5, which exhibited a small V_{str}) monotonically decreased with decreasing frequency. The amplitude of the streaming potential was also substantially larger than in the surface-orientation.

Although there is no statistically significant correlation between the amplitude of surface-oriented and deep-oriented streaming potential amplitudes at $1.0Hz$ stimulation,
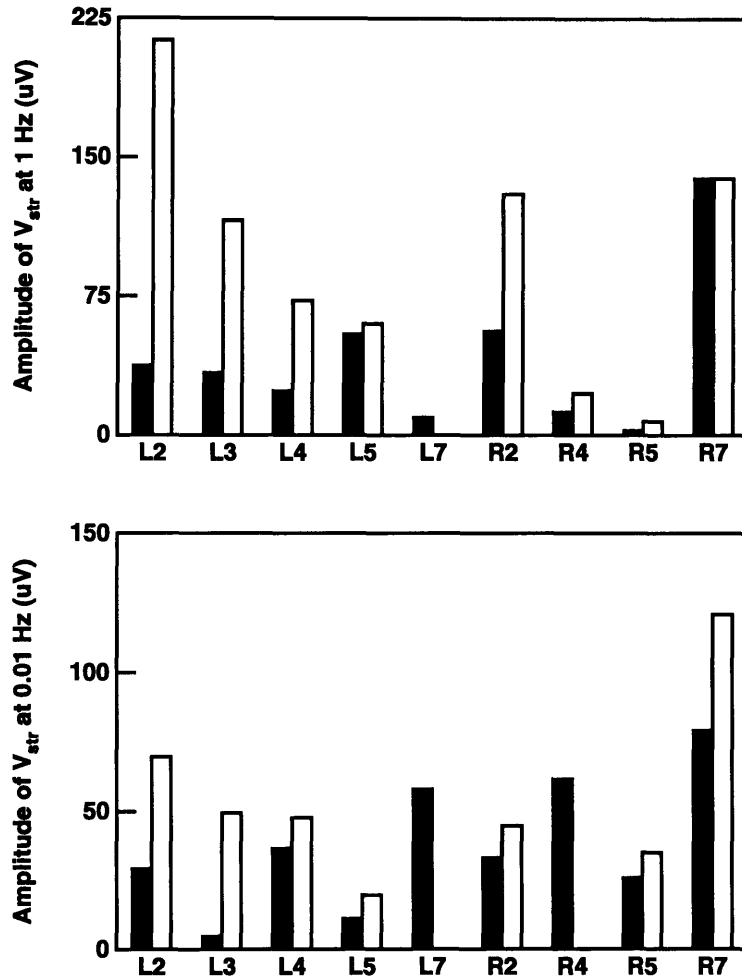
Figure 3-1: Streaming potential amplitude ($|V_{str}|$) at $1Hz$ and $0.01Hz$ for the cartilage plugs in two opposite orientations: articular surface facing porous platen (*solid bars*), and deep cartilage facing porous platen (*open bars*). L and R indicate the left or right acetabulum, with plug numbers corresponding to the core map. Some data (plugs L7 and R4) are not reported due to noisy measurements (i.e., signal was dominated by noise).
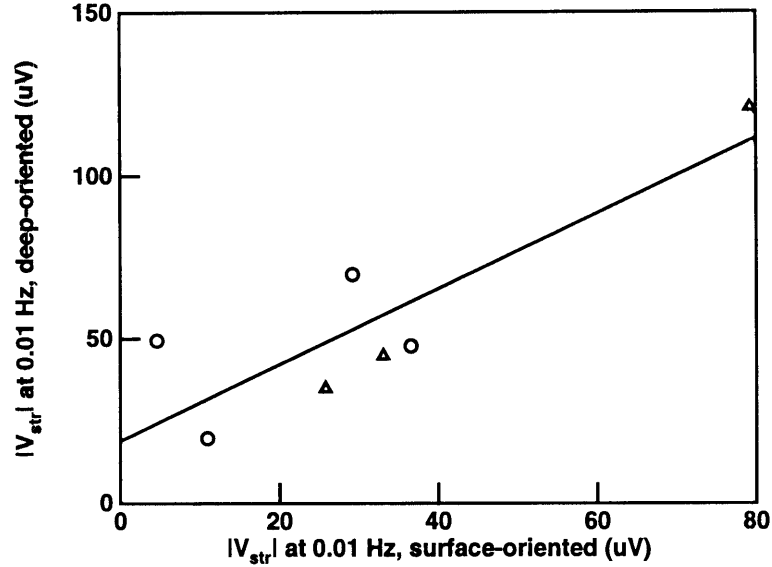
Figure 3-2: Scatter plot of low-frequency $(0.01Hz)$ $|V_{str}|$ in the surface-orientation versus in the deep-orientation. Data points are taken from both the left (o) and right ($\triangle$) acetabula. Unlike $|V_{str}|$ at $1Hz$, there is a correlation at this low frequency (line is best fit in the least squares sense).

Figure 3-2 illustrates the correlation at $0.01Hz$ $(r^2 = 0.7343, p = 0.0138)$. For all data points at $0.01Hz$, the amplitude in the deep-orientation exceeds the amplitude in the surface-orientation. It should be noted, however, that at this lower frequency the THD in the signal was typically 2–3 times larger than at $1.0Hz$, largely due to baseline drift.

3.2 Regional variations in material parameters

As seen from the streaming potential data in Figure 3-1, the behavior of the cartilage varies widely from one plug to the next (plug numbers correspond to the core map in Figure 2-1). Other compositional and material properties of the cartilage also vary with position in the acetabulum, as shown in Figures 3-3 through 3-6. The k_e and k_p values in Figures 3-6 and 3-6 are least-squares estimates obtained by non-linear fitting of the deep-orientation mechanical and electromechanical data to the model equations 1.2 and 1.3.

There is no statistically significant difference between the overall means in left and right acetabula for GAG content or any of the three material parameters. The significance level for the difference in the means (expressed as the probability that the means are identical) is
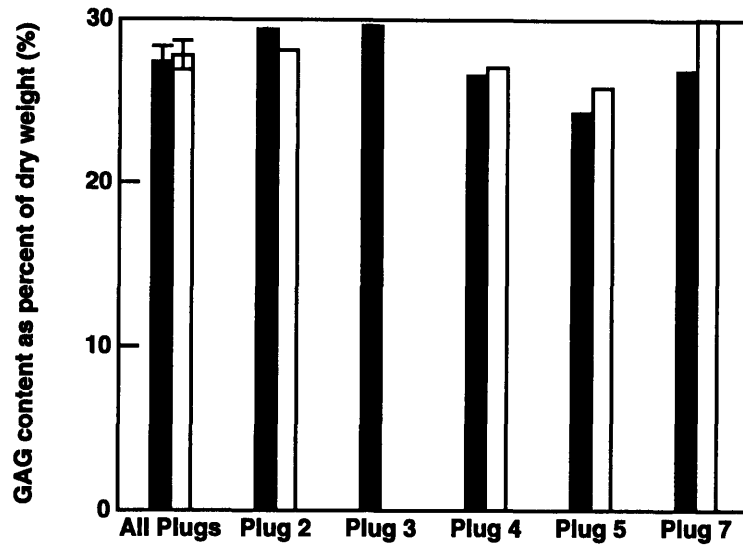
19

Figure 3-3: GAG content (by % of tissue dry weight) of the various cartilage plugs. Filled and open bars are data for left and right acetabular samples respectively. The error bars indicate standard errors of the mean when averaging all plugs from the same acetabulum.
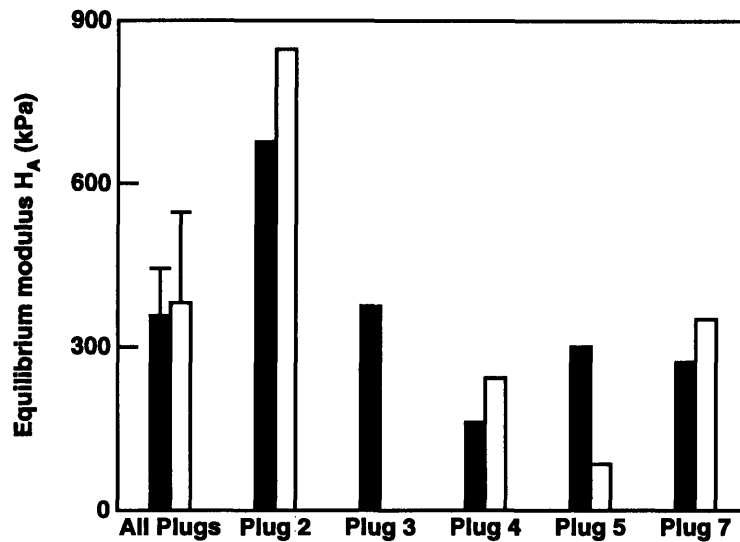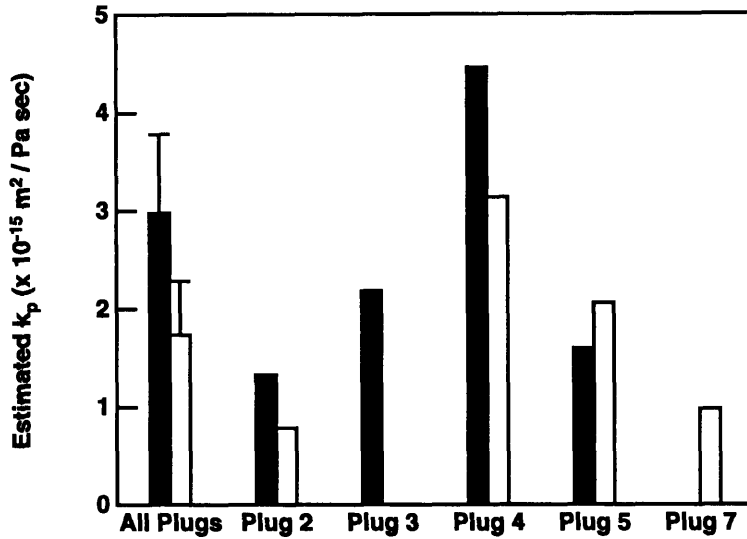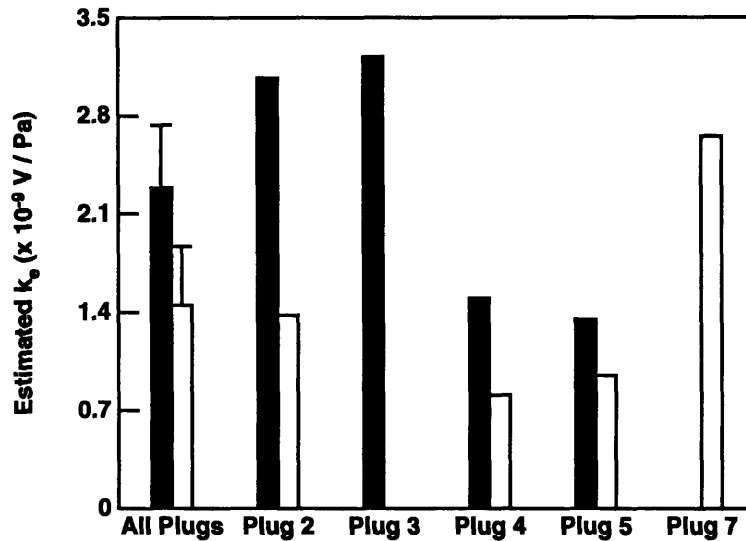

Figure 3-4: Equilibrium modulus (H_A) of the various cartilage plugs. Filled and open bars are data for left and right acetabular samples respectively. The error bars indicate standard errors of the mean when averaging all plugs from the same acetabulum.

Figure 3-5: Hydraulic permeability (k_p), as estimated from measurements in deep-orientation. Filled and open bars are data for left and right acetabular samples respectively. The error bars indicate standard errors of the mean when averaging all plugs from the same acetabulum.

Figure 3-6: Electrokinetic coefficient (k_e), as estimated from measurements in deep-orientation. Filled and open bars are data for left and right acetabular samples respectively. The error bars indicate standard errors of the mean when averaging all plugs from the same acetabulum.

Parameter	Acetabulum p-value	Location p-value
% GAG	0.89	0.77
H_A	0.76	0.044
k_e	0.14	0.23
k_p	0.46	0.091

Table 3.1: Table of significance-values for null hypothesis from 2-way ANOVA of material parameters on the variables Acetabulum (left or right) and Location (separate plug numbers).

$p = 0.25$ for k_e, and $p = 0.17$ for k_p.

Importantly, since the cores were taken from each acetabulum symmetrically with respect to the midline, the data suggest that there is more variation between regions of the same acetabulum than between the left and right acetabula. Two-way ANOVA with the factors of left/right acetabulum and plug location support this trend. Table 3.1 reports the significance levels associated with each of the calculated F statistics. With respect to the mechanical parameters H_A and k_p the location of the core is the primary source of variation. For the electromechanical parameter k_e, however, the acetabulum of origin, whether left or right, is also important. In the case of the tissue's GAG composition, however, there does not seem to be any significant trend in either factor.

3.3 Mechanical properties

An interesting relationship was observed between the theoretically estimated hydraulic permeability k_p and the observed equilibrium modulus H_A, as illustrated in Figure 3-7. The data points plotted represent both left and right acetabula as well as both surface- and deep-orientations. Irrespective of which acetabula or orientation, there appears to be a trend of decreasing permeability with increasing equilibrium modulus. This is consistent with trends previous observed in bovine tissue and in synthetic polyelectrolyte gels [29], and may be related to the dependence of these parameters on GAG and/or hydration.

The line plotted in Figure 3-7 is a linear least-squares fit to all of the data points ($r^2 = 0.389, p = 0.0075$). The data points, however, have a fairly wide range at values of H_A below $300 kPa$.
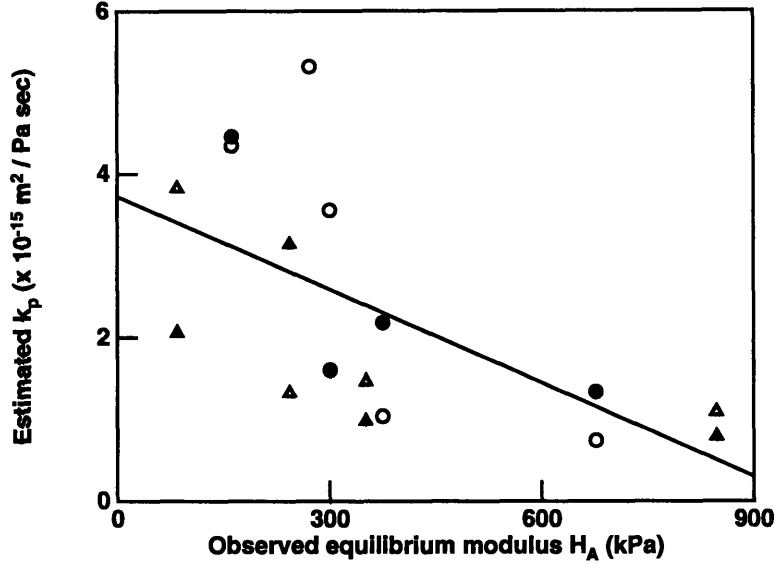
Figure 3-7: Scatter plot of k_p versus H_A, with a best-fit line. Data points are taken from both the left (o) and right ($\triangle$) acetabula, as well as in both surface- and deep-orientations (filled symbols indicate deep-oriented data). The line is fit against all of the data points.

3.4 Cartilage hydration and GAG content

The GAG content ([GAG]) of the tissue was measured as the percent fraction, by weight, of the plug's dry mass (m_{dry}). The tissue hydration H was computed as the ratio of tissue water weight to dry weight,

$$H = \frac{m_{wet} - m_{dry}}{m_{dry}}$$

As plotted in Figure 3-8, tissue hydration varied strongly with the [GAG] of the tissue. For perspective, a hydration ratio $H = 3$ would correspond to a water fraction (by weight) of 75%, while $H = 7$ corresponds to a water fraction (by weight) of 82.5%.

There was no significant (at $p = 0.05$) correlation between [GAG] and the equilibrium modulus H_A or the electromechanical variables k_e and $|V_{str}|$ in the surface-orientation. Figure 3-9 plots the correlation between increasing [GAG] and decreasing hydraulic permeability k_p ($r^2 = 0.294, p = 0.025$).

There also was a consistent trend with respect to the deep-oriented electrokinetic coefficient and streaming potential amplitude at both $1.0Hz$ and $0.01Hz$. Figure 3-10 plots this relationship for $|V_{str}|$ at $1.0Hz$ against [GAG]. Attempting a linear least-squares fit to
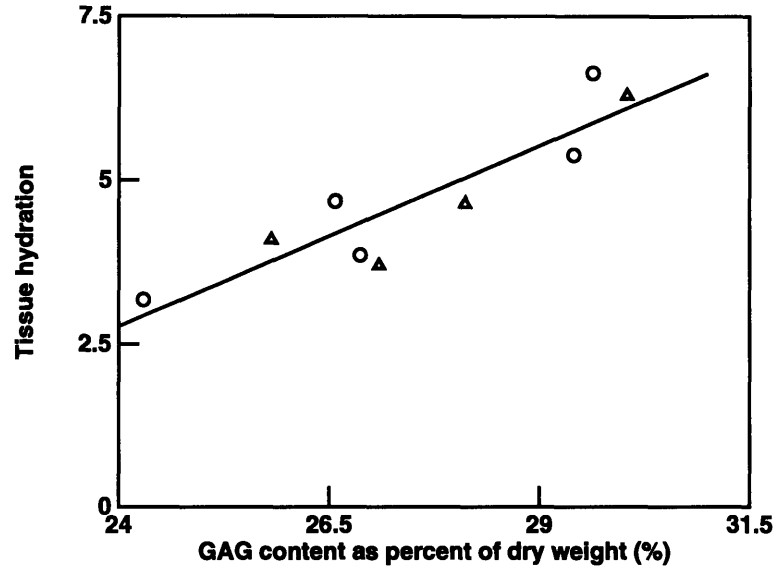
23

Figure 3-8: Scatter plot of tissue hydration H versus GAG content (% of tissue dry weight). The plotted line is best-fit against the data points, which are taken from both the left (o) and right (△) acetabula.
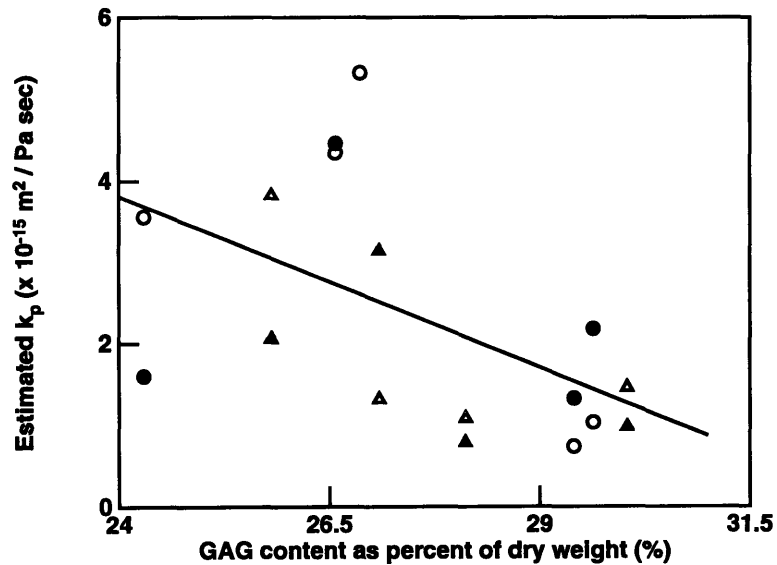

Figure 3-9: Scatter plot of hydraulic permeability versus GAG content (% of tissue dry weight). The plotted line is best-fit against the all data points, both deep-oriented (filled) and surface-oriented (open). The data plotted are from both the left (o) and right (△) acetabula.
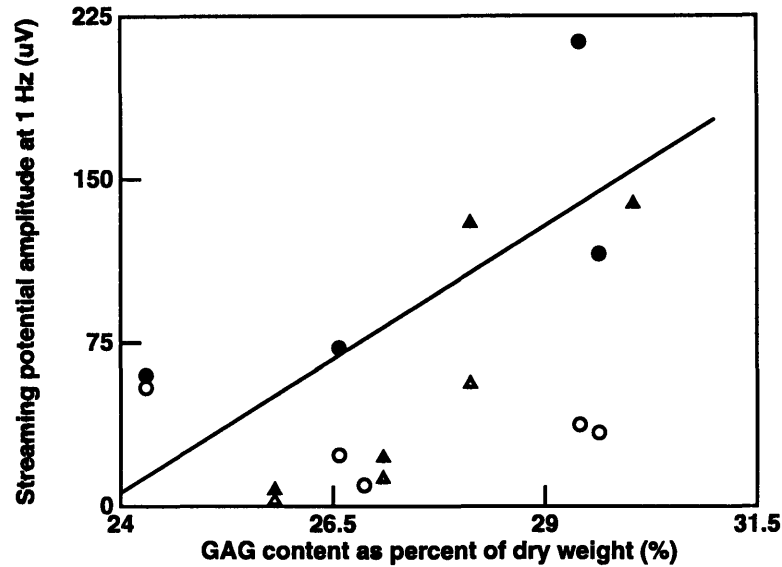
Figure 3-10: Scatter plot of $|V_{str}|$ at $1Hz$ versus GAG content (% of tissue dry weight). The plotted line is best-fit against the deep-oriented data points only (filled points). The data plotted are from both the left (o) and right ($\triangle$) acetabula in both deep- and surface-orientations.

the data in Figure 3-10 gives an $r^2 = 0.543$ ($p = 0.037$), although the trend in the data appears to be higher order. A remarkably similar trend also occurs with respect to both the low-frequency ($0.01Hz$) streaming potential and the estimated electrokinetic coefficient, the latter of which is plotted in Figure 3-11 ($r^2 = 0.625$, $p = 0.020$). Again, the values of k_e estimated in the deep-orientation has a clear trend with increasing [GAG], while k_e estimated in the surface-orientation has no correlation.

Interestingly, the tissue hydration H appeared to increase faster than linearly with respect to the tissue GAG content. Figure 3-12 plots [GAG] versus the ratio of [GAG] to H. This ratio appears to decrease as the GAG content increases. Accordingly, if GAG content is measured as a percent fraction of tissue *wet* weight, the streaming potential amplitude and k_e actually decrease with an increasing GAG % of wet weight, as illustrated in Figures 3-13 and 3-14.
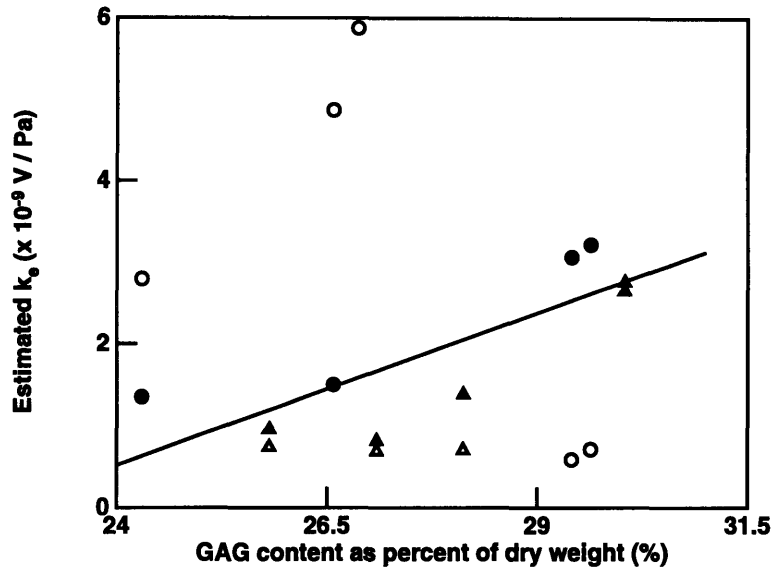
25

Figure 3-11: Scatter plot of k_e versus GAG content (% of tissue dry weight). The plotted line is best-fit against points estimated from deep-oriented data only (filled points). The data plotted are from both the left (o) and right (△) acetabula in both deep- and surface-orientations.
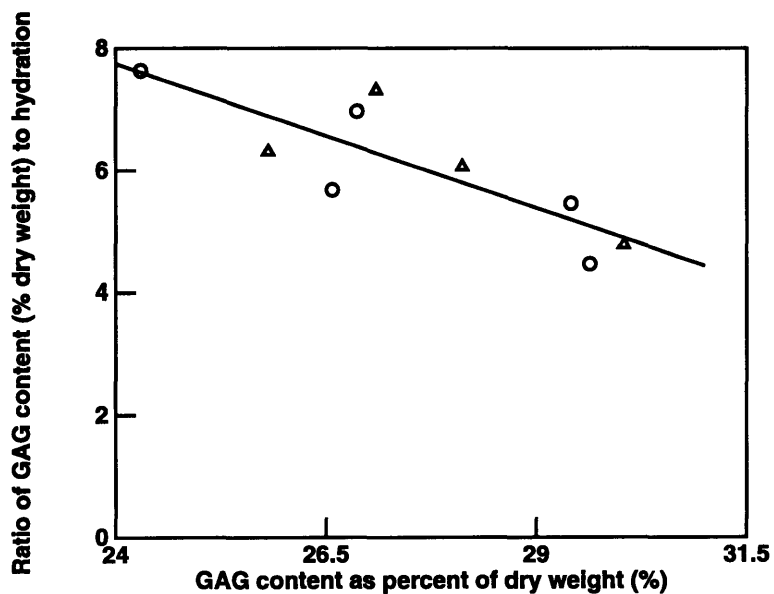

Figure 3-12: Scatter plot of the ratio of [GAG] to hydration versus [GAG] (% of tissue dry weight). The plotted line is best-fit against all data points. The data plotted are from both the left (o) and right (△) acetabula.
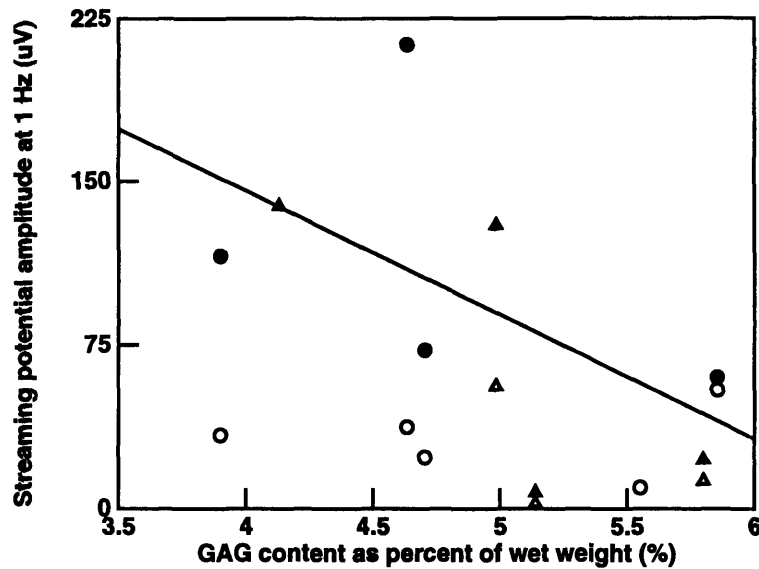
Figure 3-13: Scatter plot of $|V_{str}|$ at $1Hz$ versus GAG content (% of tissue wet weight). The plotted line is best-fit against the deep-oriented data points only (filled points), and does not meet a significance test ($p = 0.1220$). The data plotted are from both the left (o) and right ($\triangle$) acetabula in both deep- and surface-orientations.
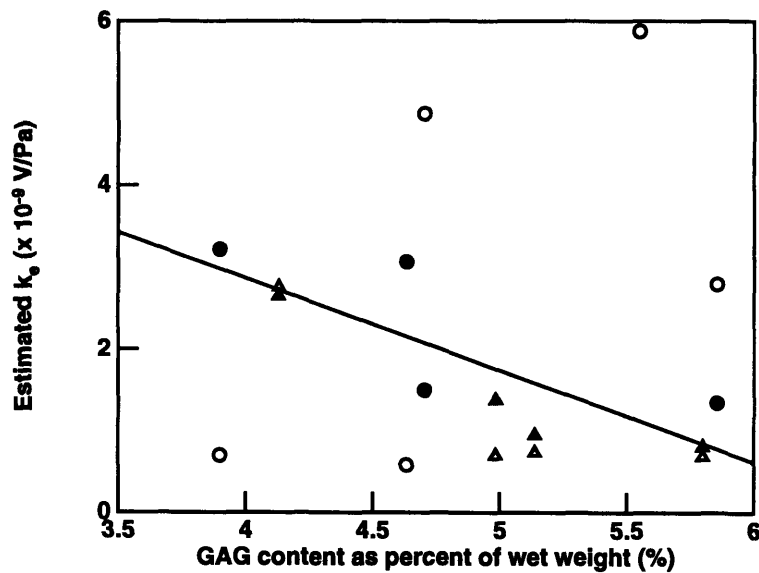

Figure 3-14: Scatter plot of k_e versus GAG content (% of tissue wet weight). The plotted line is best-fit against points estimated from deep-oriented data only (filled points). The data plotted are from both the left (o) and right ($\triangle$) acetabula in both deep- and surface-orientations.
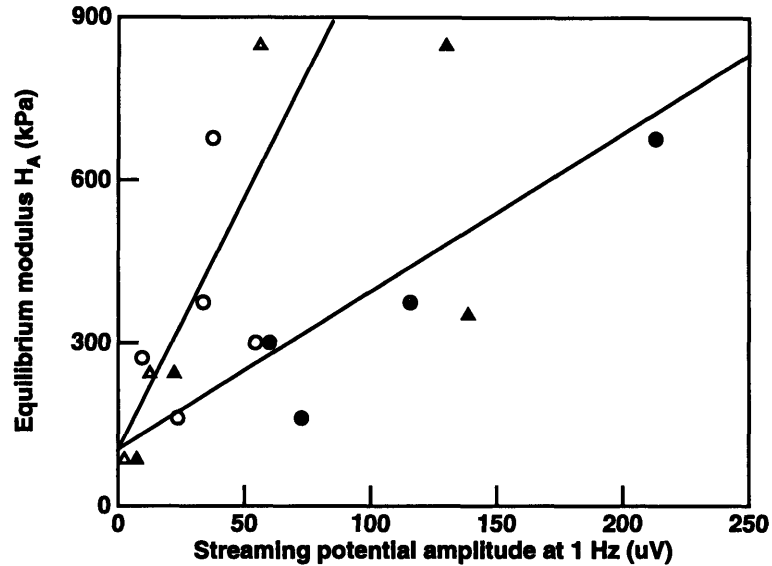
27

Figure 3-15: Scatter plot of equilibrium modulus H_A versus streaming potential amplitude at $1Hz$. The two plotted lines are best-fit against the surface-oriented and deep-oriented populations. Data points are taken from both the left (o) and right ($\triangle$) acetabula, as well as in both surface- and deep-orientations (filled symbols indicate surface-oriented).

3.5 Streaming potential as an evaluator of cartilage

Figure 3-10, viewed in the reverse sense of [GAG] as a function of streaming potential, illustrates how an electromechanical measurement might be used to estimate the properties of the cartilage specimen. Given a streaming potential measurement, the correlation allows one to estimate the GAG content of the tissue or tissue hydration.

Figure 3-15 further addresses the feasibility of using electromechanical measurements like the streaming potential as a clinical tool for cartilage evaluation. In both surface- and deep-orientations there is an approximately linear correlation between the observed streaming potential amplitude (reported at $1.0Hz$) and the tissue's equilibrium modulus.

Both the surface-oriented best-fit line ($r^2 = 0.515$, $p = 0.045$) and the deep-oriented best-fit line ($r^2 = 0.581$, $p = 0.028$) represent fairly strong correlations. Notably, the two lines approximately intersect when $|V_{str}|$ goes to zero, converging at an ordinate-intercept of $103-104kPa$. The slope of the surface-oriented line is 3.20 times greater than the slope of the deep-oriented line.

Chapter 4

Discussion

4.1 Dependence upon orientation

The poroelastic nature of cartilage ensures that a small sinusoidal strain imposed on one surface will not uniformly deform the tissue throughout its thickness. At high frequencies, fluid flow is constrained to the surface of the tissue. At low frequencies, the tissue is more able to relax, and fluid flow occurs throughout the bulk of the tissue.

The theoretical model for streaming potentials in confined compression thus predicts that, at high frequencies, the streaming potential will depend largely on the tissue's properties near the porous boundary. At low frequencies, the streaming potential will then become sensitive to the properties of tissue zones farther from the porous boundary condition. The observed data strongly support the hypothesis that we have tested an inhomogenous tissue whose properties near the surface are remarkably different from the properties in the deeper cartilage. It will be important to see if this hypothesis is supported by histological assessment of the tissue from these acetabula (in progress).

From the streaming potential results (Figure 3-1), it appears that the articular surface of the cartilage has a weaker transduction between mechanical and electrical phenomena. This reduction could be due to several factors reported in the literature [26]. Specifically, it has been observed that collagen fibrils near the surface run tangentially to the surface, while fibrils in the middle and deep zones exhibit a random orientation; however, the removal of $\sim 50\mu m$ of surface cartilage to planarize the plug may have also eliminated this tangential

29

surface layer. Cartilage hydration has been reported to be highest in the upper 20% of the surface, falling roughly from a water fraction (w/w) of 80% to 70% ($H = 4.0$ to $H = 2.3$) in deeper zones of cartilage. Finally, it has also been shown that GAG concentrations are lowest at the cartilage surface and rise with increasing depth in adult tissue.

These factors may result in the observed differential between surface-oriented and deep-oriented responses. Increased hydration near the surface of the tissue physically implies an increased permeability, which affects both the electrokinetic coefficient k_e as well as the dynamic modulus and fluid velocity. The fixed charge concentration near the surface may also be smaller than in the bulk of the tissue, thus reducing the coupling between mechanical and electrical flows.

The presence of this inhomogeneity presents a difficulty in modelling the tissue. Equation 1.3 predicts a monotonically decreasing streaming potential as the frequency decreases, contrary to observations of several surface-oriented plugs. Multi-layer or finite element models of the tissue would be necessary to properly account for such tissue inhomogeneities [19].

For the range of H_A and k_p observed in this study, the corresponding value for γ^{-1} is on the order of $20\mu m$ at $1.0Hz$ and $200\mu m$ at $0.01Hz$. Fluid velocities, in theory, exponentially fall to zero on a depth scale of 3–5 skin depths. Accordingly, the streaming potentials at $1.0Hz$ most strongly reflect material properties very near ($\sim 100\mu m$) the porous boundary. The lack of correlation between surface-oriented streaming potentials and GAG content (see Figure 3-10) suggests that these electrokinetic properties of the articular surface are, to first-order, independent of the whole tissue GAG content. The correlation between deep-oriented $1.0Hz$ streaming potentials and GAG content, however, suggests the opposite. That is, the tissue's inhomogeneity may be largely restricted to the articular surface, while the transitional and deep zones are fairly homogeneous with respect to gross electromechanical behavior. It will be interesting to interpret these results in light of the cartilage specimens' histological findings.

4.2 Mechanical parameters

It is interesting to note that the inverse relationship between H_A and k_p (Figure 3-7) appears to hold true independent of which acetabulum (left or right) and the location within the acetabulum. Thus while the absolute magnitude of these parameters vary greatly within the acetabulum, these parameters do not appear to be independent of one another. Instead, they are dependent upon one or more intrinsic properties of the cartilage tissue.

In vivo cartilage stresses were previously measured in an implanted endoprosthesis study of a 73-year old woman [22]. Stresses measured during dynamic activity like rising from a chair reached as high as $15MPa$. During the stance phase of walking, contact pressures typically reached 1–3 MPa across the acetabulum. For comparison, cartilage in this study under dynamic strains of 1% at $0.01Hz$ had a dynamic compressive stiffness ranging from 0.6 to $4.2MPa$. The dynamic stiffness at $1.0Hz$ ranged from 1.0 to $7.8MPa$ (see Table A.2 in the Appendix).

The observed values of H_A and k_p are smaller than, but of a similar order of magnitude as values previously reported for adult bovine articular cartilage and human patellar cartilage. Frank and Grodzinsky (1987b), using uniaxial confined compression experiments, found $H_A = 990kPa$ and $k_p = 3 \times 10^{-15}m^2/Pa\ sec$ in bovine femoropatellar cartilage equilibrated in $1mM$ NaCl. Eisenberg and Grodzinsky (1985) found that H_A decreased to $550kPa$ when equilibrated at $0.15M$ NaCl. Mow et al. (1980), measuring the creep response of bovine cartilage plugs in confined compression, estimated material values of $H_A = 700kPa$ and $k_p = 7.6 \times 10^{-15}m^2/Pa\ sec$. Armstrong and Mow (1982) measured the creep response of human patellar cartilage from 103 patients aged 16 to 85, and found a wide range of permeability (mean of $4.7 \times 10^{-15}m^2/Pa\ sec$) and modulus (mean of $790kPa$).

Athanasiou et al. (1994) employed indentation tests on 10 pairs of healthy human femoral heads and acetabula to numerically estimate the cartilage mechanical parameters. Their observed values of H_A in the acetabula ranged from $1.072MPa$ to $1.424MPa$ depending uon location in the acetabulum, although with substantial standard deviations for each location ($\sim 0.5MPa$). Their estimated hydraulic permeability values ranged from

0.710×10^{-15} to $1.133 \times 10^{-15} m^2/Pa$ sec, again with substantial standard deviations. Thus our cartilage tissue was generally softer and more permeable than the acetabular cartilage tested by Athanasiou et al. (1994).

4.3 Electromechanical properties

The estimated deep-orientation values of k_e, on the order of $10^{-9} V/Pa$, are an order of magnitude smaller than the $2 \times 10^{-8} V/Pa$ values reported in adult bovine tissue by Frank and Grodzinsky (1987b). However, in that study a low ionic strength bath ($1mM$ NaCl) was employed, implying that the Debye length and, correspondingly, electrostatic interactions would be greater than at more phyiologic ionic strengths. For example, a 3-fold decrease in the streaming potential amplitude has been reported when the bath ionic strength is raised from $1mM$ to $100mM$ [16]. The remainder of the variation can be partially attributed to the decreased stiffness and increased permeability of this human tissue relative to bovine tissue, which alters the fluid flows resulting from an applied dynamic strain.

The electromechanical results show a fairly strong positive correlation between streaming potential amplitude or k_e and the GAG content of the tissue (measured as % of dry weight). This result is consistent with previous reports that the ionized acid groups of the GAG molecules are the principal substrate for electrokinetics.

However, in continuum theories of cartilage electrokinetics [11] it is the space charge density and spatial GAG concentration that governs the magnitude of the electromechanical transduction, not just the proportion of GAG in the solid tissue. We have observed, however, that as the GAG % dry weight increases, the tissue hydration increases at an even faster pace. As the amount of GAG relative to other tissue solid components increases, the spatial GAG concentration (approximately measured as GAG % wet weight) decreases. Figures 3-13 and 3-14 show that as the spatial concentration of GAG decreases we observe a larger, not smaller, streaming potential and k_e.

4.4 Tissue hydration and GAG content

A negative correlation was also observed between tissue hydration and hydraulic permeability, as confirmed in Figure A-2 in the Appendix. It would normally be expected that increasing hydration (as a result of swelling) would correlate with increased hydraulic permeability and decreased equilibrium modulus and V_{str} [1].

Figure 4-1 graphs, as a function of tissue hydration, the whole-tissue wet weight, dry weight, GAG weight, and thickness (data from Table A.1 in the Appendix). With hydration increasing from approximately 3 to 7, the trends in these tissue properties are qualitatively summarized in Table 4.1.

Property	Approx. net change (% of value at $H \simeq 3$)	Rating
Total wet weight	-10%	$-$
Total dry weight	-50%	$-\,-\,-$
Total GAG weight	-35%	$-\,-$
Thickness (neglecting outliers)	$+25\%$	$+$
GAG % dry weight		$+$
GAG % wet weight		$-$

Table 4.1: Approximate net changes in total tissue weights and thickness as hydration increased from $H \simeq 3$ to $H \simeq 7$.

From these trends we can conclude that increasingly hydrated plugs had decreased amounts of solid matrix, an increased proportion of GAG in the solid matrix, and a slightly decreased wet weight. These observations are consistent with the hypothesis of a weakened collagen matrix, as the loss of collagen would increase the proportion of GAG in the dry mass. Thickness and wet weight may change to a smaller degree as a result of physiological remodelling. The long-term stress history experienced by a region of cartilage would depend upon its articulation with the femoral head, and thus its thickness. As cartilage volume is principally occupied by water, the wet weight may then be simultaneously regulated by physiological processes.

It is possible that certain portions of this patient's acetabular cartilage had lost extracellular matrix over time due to aging or disease. The increasing GAG % dry weight may then represent a disease process more specific to collagen, or increased physiological synthesis
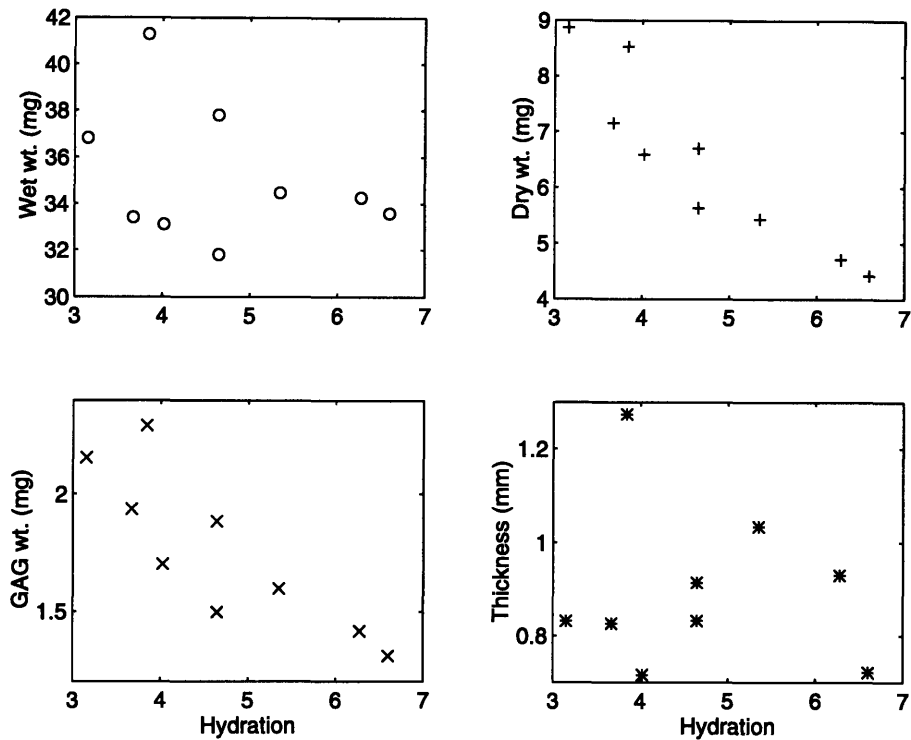
Figure 4-1: Scatter plots of total tissue weights (wet, dry, and GAG) and thickness versus hydration.

of GAG in an attempt to maintain cartilage functionality.

4.5 Damaged extracellular matrix

Cartilage H_A and $|V_{str}|$ have been reported in tissue that has been enzymatically or surgically modified. Frank et al. (1987c) digested bovine cartilage with both chondroitinase-ABC and trypsin. In both cases, the enzymatic digestion of glycosaminoglycan chains over several hours resulted in a simultaneous decrease in both H_A and $|V_{str}|$. Bonassar et al. (1995) digested bovine cartilage in stromelysin I (matrix metalloprotease 3), which is known to deplete cartilage of GAG as well as cleave type IX collagen and clip type II collagen within the non-helical (telopeptide) region [6, 12]. When 90% of the tissue GAG had been depleted by stromelysin I digestion, the H_A decreased by 90%, the k_p increased by a factor of 15, and the streaming potential at $1Hz$ decreased by 90%. Hoch et al. (1983) surgically performed medial meniscectomies in rabbits and observed a 60% decrease in H_A, a 160% increase

34

in k_p, and a 55% decrease in streaming potential. The alterations in Hoch et al. (1983) correlated with increases in tissue hydration. In Bonassar et al. (1995), weakening of the collagen framework was explicitly implicated during stromelysin treatment. Cartilage samples digested in trypsin or chondroitinase ABC, which selectively remove GAG, showed no swelling when transferred from physiologic saline to $0.01M$ saline. Cartilage digested in stromelysin, however, did swell by approximately 25%.

These previous results suggest that damage to the collagen matrix results in increased hydration of the tissue, while loss of glycosaminoglycans results in the decreased H_A and $|V_{str}|$. Since the hydration in this study is observed to strongly increase with increasing GAG % dry weight, we suggest that the collagen matrix may be damaged or weakened in some of these cartilage specimens, allowing swelling to occur. Figure 3-12 then indicates that this swelling increases faster than linearly with GAG % dry weight.

Taken alone, the correlations between H_A, k_p, V_{str}, and k_e are consistent with previous studies in which cartilage was altered enzymatically or surgically. Likewise, taken alone, it is possible to postulate simple mechanisms for the trends in hydration, dry weight, and wet weight. We reach a contradiction, however, if we equate GAG % wet weight with GAG fixed charge density and thus attempt to relate the tissue's biochemical properties with the observed electromechanical behavior. There is no contradiction if we take GAG % dry weight to be a more reliable indicator of space charge density.

It is possible that several factors involving collagen, GAG, and other tissue components interact in a complex way to produce the contradiction in correlations with GAG % wet weight. For example, perhaps some plugs had a low content of collagen or network damage in the superficial cartilage zone, thus increasing the aggregate GAG % dry weight and allowing a higher degree of swelling in the surface zone. The equilibrium modulus may then still be appreciable at a 15% static strain as the middle and deep zones of cartilage have an intact collagen matrix and correspondingly high fixed charge density. The deep-oriented streaming potentials, electrokinetic coefficients, and hydraulic permeabilities, being primarily sensitive to the cartilage properties near the deep-zone, would not strongly reflect the weakened collagen matrix at the surface. Although this hypothesis can not be proven or disproven with the data collected in this study, it illustrates the large number

of factors that may come into play. More detailed studies, quantifying collagen integrity and the variation with depth in biochemical and electromechanical properties, would be necessary to answer these questions.

4.6 Electrokinetic evaluation of cartilage

There are several clinical goals of research in cartilage electromechanics. Understanding of cartilage electromechanics would shed light on the normal mechanical function of cartilage, as well as on potential regulatory and signalling mechanisms for cartilage remodelling and disease. A more immediate goal is the use of cartilage electromechanics to non-destructively and practically evaluate the health of a person's articular cartilage.

Figure 3-10 suggests that the amplitude of the streaming potential is also an indicator of the tissue's glycosaminoglycan content, in at least this patient's acetabula. The correlation is independent of the acetabula of origin and the position within the acetabula, suggesting that we are truly measuring material properties. In light of the discussion in the previous section regarding the GAG % dry weight versus GAG % wet weight results, several material properties may influence the relationship between GAG and streaming potential. When used as just one of several indicators in clinical diagnosis, however, this variation may not be important. A large scale investigation, involving many human subjects, would be useful in describing the limits of "normal behavior," and highlighting commonalities in pathological cartilage.

Significantly, the two parameters plotted in Figure 3-15 are both directly measured, and not numerically estimated given a theoretical model. A trend clearly exists between increased equilibrium moduli and streaming potential amplitude. The fact that the two trends intercept the H_A axis at the same point strongly suggests a conceptual model in which cartilage has a baseline compressive modulus that is augmented by electromechanical effects.

Eisenberg and Grodzinsky (1985) measured H_A in bovine articular cartilage over a range of bath ionic strengths. At a very low ionic strength ($0.005M$ NaCl), the equilibrium modulus was found to be $1.1MPa$. In physiologic saline ($0.15M$ NaCl), H_A decreased to

$0.55MPa$. H_A was almost identical at $0.5M$ and $1.0M$ NaCl; at $1.0M$ NaClthe reported modulus is $0.27MPa$. This decrease in equilibrium modulus was attributed to the ionic shielding of the electrostatic effects. In a binary electrolyte, for example, the Debye length decreases as the square root of the bath ionic strength.

These results are consistent with the results of this present study. The solid components of the extracellular matrix will have some intrinsic modulus, while the electrostatic repulsion and osmotic pressure of the fixed charge density adds a significant resistance to equilibrium compression. The differing slopes of the two trends in Figure 3-15 may be produced by a variety of factors, as discussed previously with respect to cartilage orientation.

These results demonstrate that the streaming potential measurements in confined compression are indeed correlated with functional properties important in load-bearing. It is important to recall that this study involved cartilage samples from just one patient, thus precluding generalized conclusions. However, in at least this study a non-destructive electromechanical measurement of human cartilage conveyed information regarding material properties like equilibrium modulus and glycosaminoglycan content.

Confined compression streaming potentials, however, would be inappropriate in a clin-ical setting. Although non-destructive, the *in vitro* testing protocol requires explantation of cartilage and electrical access to both the articular surface and deep-zones of the cartilage. Recently, a new measurement modality has been implemented in which small, spatially-varying currents are injected into the articular surface of the cartilage and the resultant spatially-varying electromechanical stresses are measured. This electromechanical surface spectroscopy [3, 5] has the potential for *in vivo* arthroscopic use, making it an attractive, minimally invasive technique. It remains to be seen in further experiments whether that modality can likewise elicit information about health and functional properties in human articular cartilage.

Appendix A

Data

This appendix consists of three sections. The first section is a tabular listing of the principal data collected in this study. The second section catalogs scatter plots of H_A, k_p, $|V_{str}|$ at $1.0Hz$, and k_e against several material parameters of the tissue: GAG content as percent of dry weight, GAG content as percent of wet weight, and tissue hydration H. The third section catalogs scatter plots of GAG content (as % of dry weight), tissue hydration, H_A, and k_p against the observed streaming potential amplitudes, at either $1.0Hz$ or $0.01Hz$. The data in the plots are not mutually exclusive, e.g. with diligence one could identically construct a plot of H_A vs. $|V_{str}|$ using data from scatter plots of H_A vs. H and $|V_{str}|$ vs. H.

In each plot data points from both left and right acetabula are used. Data points are marked with (○) symbols for the left acetabulum, and with (△) symbols for the right acetabulum. When appropriate (i.e., for k_p, k_e, and $|V_{str}|$) the data are further split by plug orientation, whether surface-oriented (clear points) or deep-oriented (filled points).

For each plot an attempt was made to linearly correlate the abscissa and ordinate parameters. When the data did correlate with $p < 0.05$ a best-fit line is also plotted; the absence of a line indicates a lack of statistically significant correlation. The figure caption describes the data set to which the line was fit and the corresponding r^2 and p values; in some cases all data points were used, while others use only the deep-oriented data. Figure A-17 plots two lines, one each for the deep- and surface-oriented data sets.

Core No.	Thickness [μm]	Wet wt. [mg]	Dry wt. [mg]	GAG wt. [mg]	H_A [kPa]	k_p ($\times 10^{-15}$) [$m^2/Pa\ sec$]	k_e ($\times 10^{-9}$) [V/Pa]
Surface							
Left 2	1034	34.47	5.43	1.60	676.9	0.74	0.58
Left 3	722	33.59	4.42	1.31	375.1	1.03	0.71
Left 4	832	31.80	5.63	1.50	162.0	4.35	4.87
Left 5	831	36.81	8.87	2.15	300.6	3.56	2.80
Left 7	1274	41.29	8.53	2.29	272.3	5.32	5.88
Right 2	914	37.80	6.70	1.88	847.4	1.09	0.70
Right 4	826	33.40	7.15	1.94	243.2	1.32	0.69
Right 5	716	33.10	6.59	1.70	84.6	3.82	0.74
Right 7	930	34.26	4.71	1.41	351.4	1.46	2.76
Deep							
Left 2	1034	34.47	5.43	1.60	676.9	1.33	3.07
Left 3	722	33.59	4.42	1.31	375.1	2.18	3.22
Left 4	832	31.80	5.63	1.50	162.0	4.46	1.50
Left 5	831	36.81	8.87	2.15	300.6	1.60	1.35
Right 2	914	37.80	6.70	1.88	847.4	0.79	1.38
Right 4	826	33.40	7.15	1.94	243.2	3.14	0.81
Right 5	716	33.10	6.59	1.70	84.6	2.06	0.95
Right 7	930	34.26	4.71	1.41	351.4	0.98	2.65

Table A.1: Summary of data in both surface- and deep-orientations.

Core No.	Dynamic Mod. [MPa]		Mag(Str. pot.) [uV]	
	[$1Hz$]	[$0.01Hz$]	[$1Hz$]	[$0.01Hz$]
Surface-oriented				
Left 2	5.25	3.35	37.39	29.21
Left 3	2.91	1.70	33.70	4.59
Left 4	1.96	0.93	23.55	36.57
Left 5	1.92	1.10	54.34	10.97
Left 7	2.84	1.50	9.60	58.11
Right 2	7.82	3.90	56.07	33.07
Right 4	3.43	1.88	12.57	61.73
Right 5	0.96	0.61	2.51	25.81
Right 7	4.63	2.35	138.60	79.24
Deep-oriented				
Left 2	5.08	3.02	213.00	69.71
Left 3	3.09	1.53	115.70	49.42
Left 4	1.48	0.78	72.58	47.72
Left 5	3.86	2.07	59.99	19.70
Right 2	7.60	4.15	129.80	44.75
Right 4	3.25	-n/a-	22.27	-n/a-
Right 5	1.83	1.04	7.44	34.87
Right 7	5.94	2.85	138.60	121.00

Table A.2: Summary of data in both surface- and deep-orientations.
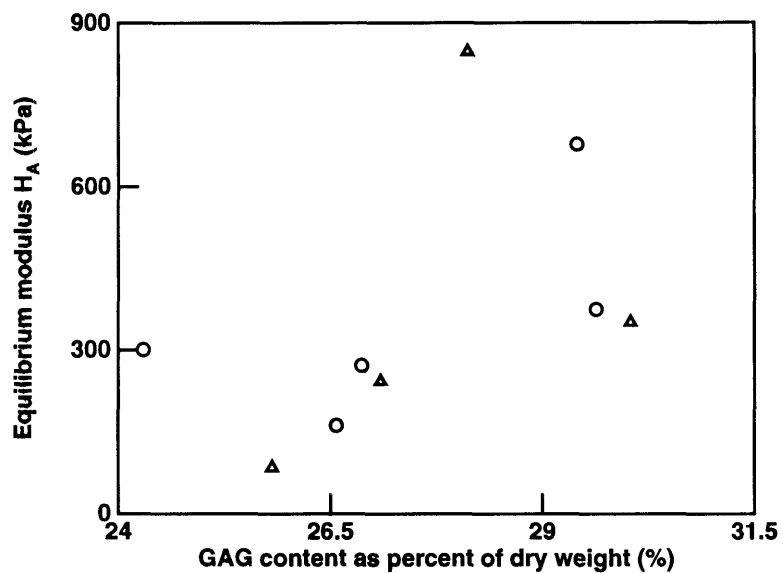
Figure A-1: Scatter plot of H_A versus [GAG] (as % of dry weight).
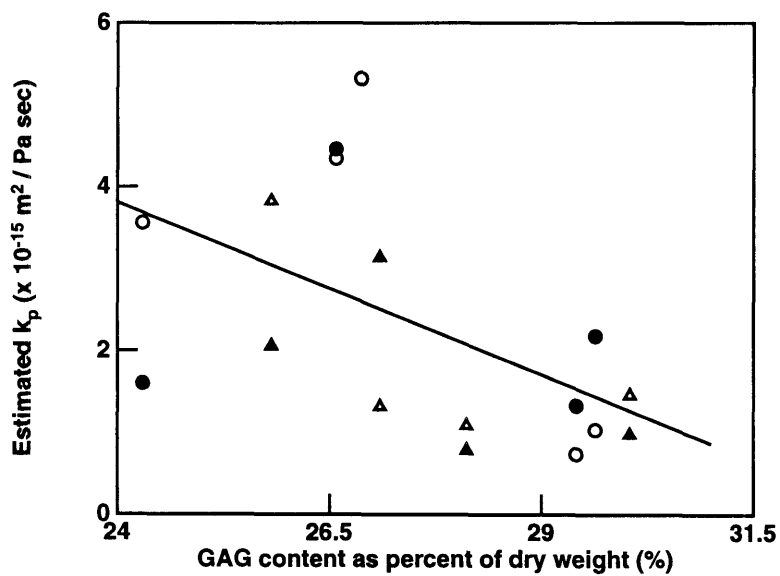
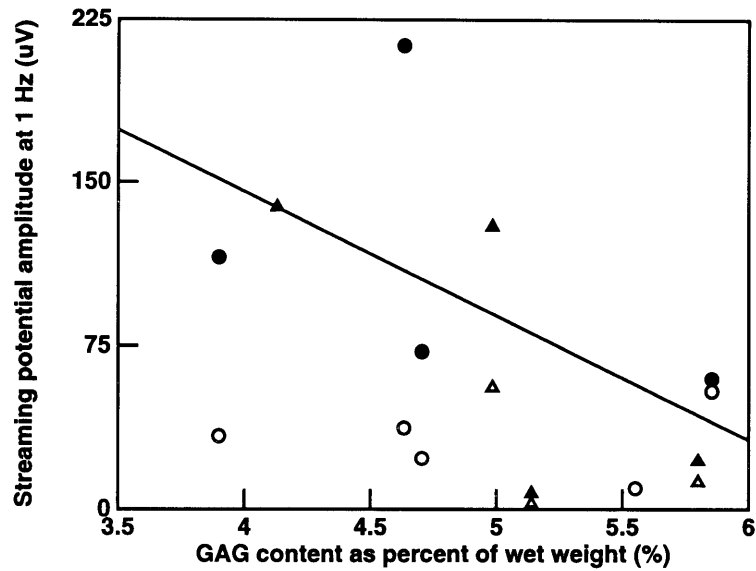Figure A-2: Scatter plot of k_p versus [GAG] (as % of dry weight). Line is fit against all data points, $r^2 = 0.294, p = 0.025$.
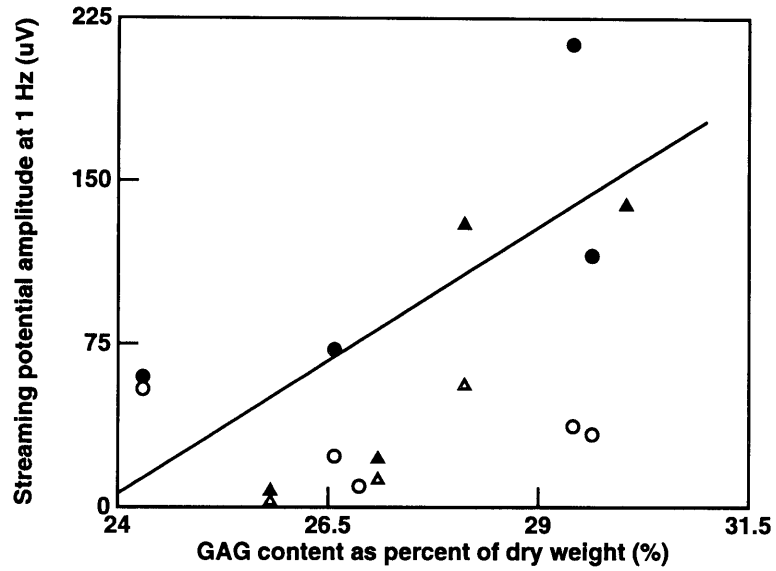
Figure A-3: Scatter plot of $|V_{str}|$ at $1.0Hz$ versus [GAG] (as % of dry weight). Line is fit against the deep-oriented data points only, $r^2 = 0.543, p = 0.037$.
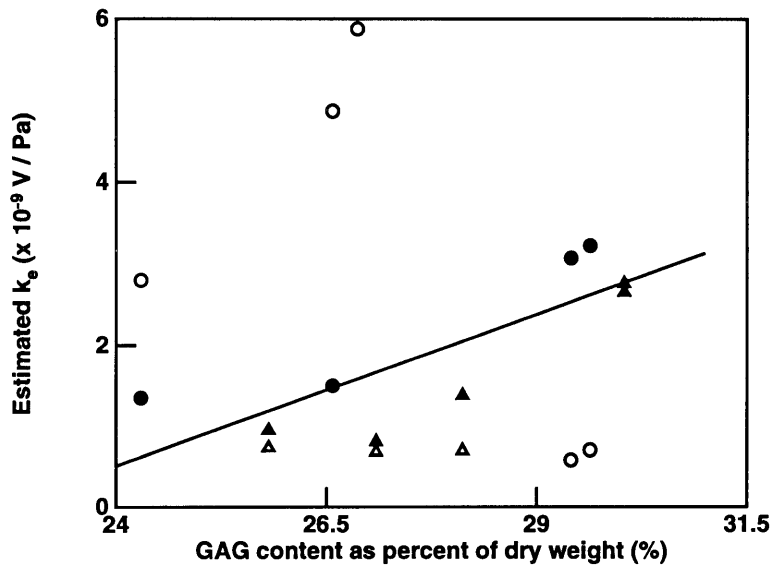
Figure A-4: Scatter plot of k_e versus [GAG] (as % of dry weight). Line is fit against deep-oriented data points only, $r^2 = 0.625, p = 0.020$.
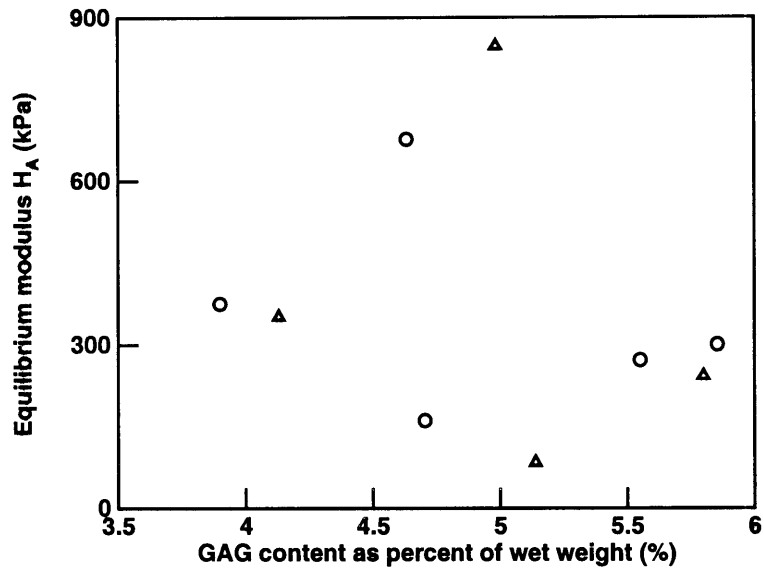
Figure A-5: Scatter plot of H_A versus [GAG] (as % of wet weight).
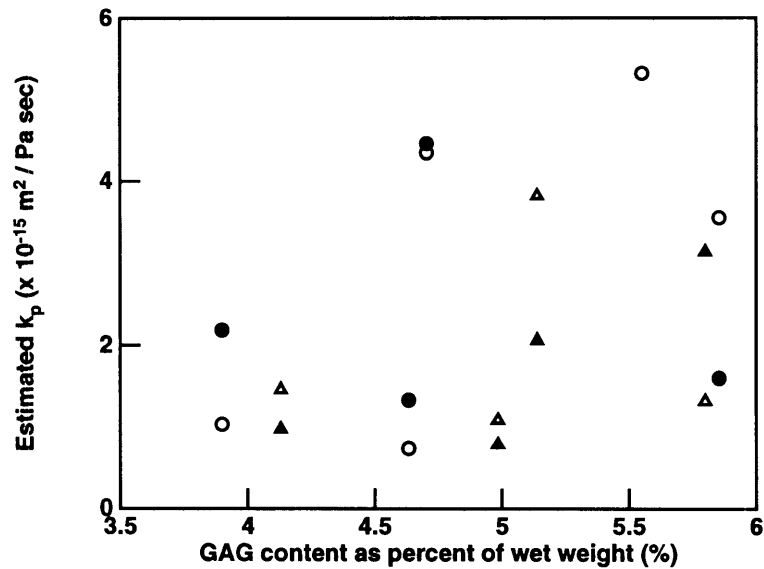
Figure A-6: Scatter plot of k_p versus [GAG] (as % of wet weight).

Figure A-7: Scatter plot of $|V_{str}|$ at $1.0Hz$ versus [GAG] (as % of wet weight). Line plotted is for illustration purposes, and was best-fit against the deep-oriented data points only, $r^2 = 0.351, p = 0.12$.
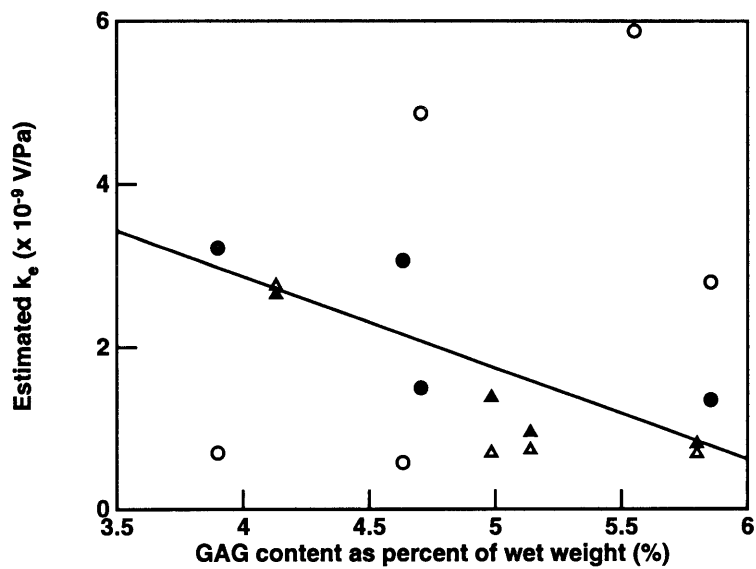
Figure A-8: Scatter plot of k_e versus [GAG] (as % of wet weight). Line is fit against deep-oriented data points only, $r^2 = 0.676, p = 0.012$.
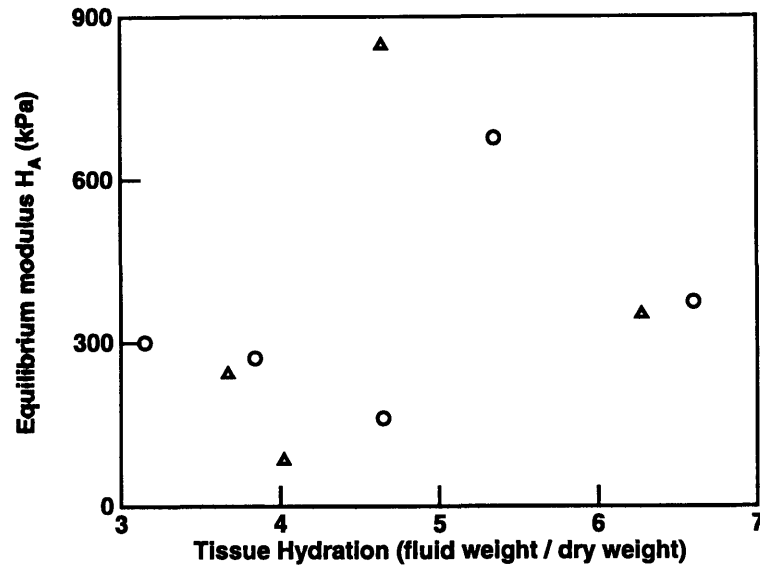
Figure A-9: Scatter plot of H_A versus hydration (ratio of fluid weight to dry weight).
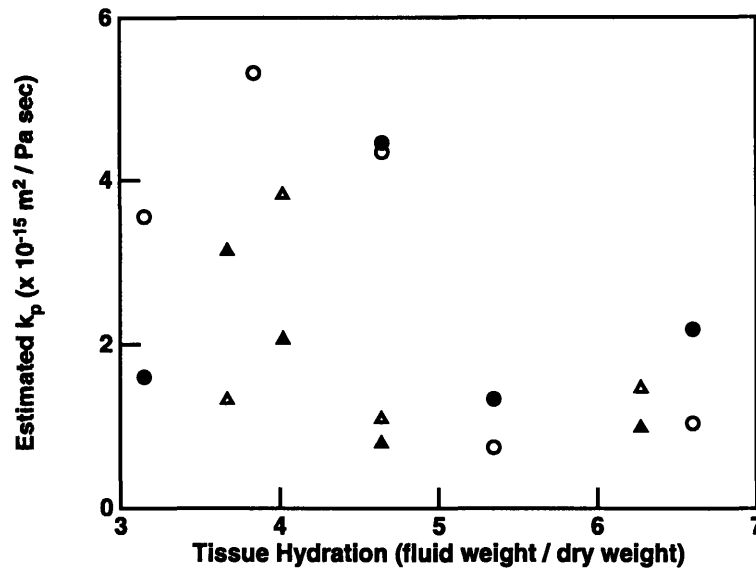
Figure A-10: Scatter plot of k_p versus hydration (ratio of fluid weight to dry weight).
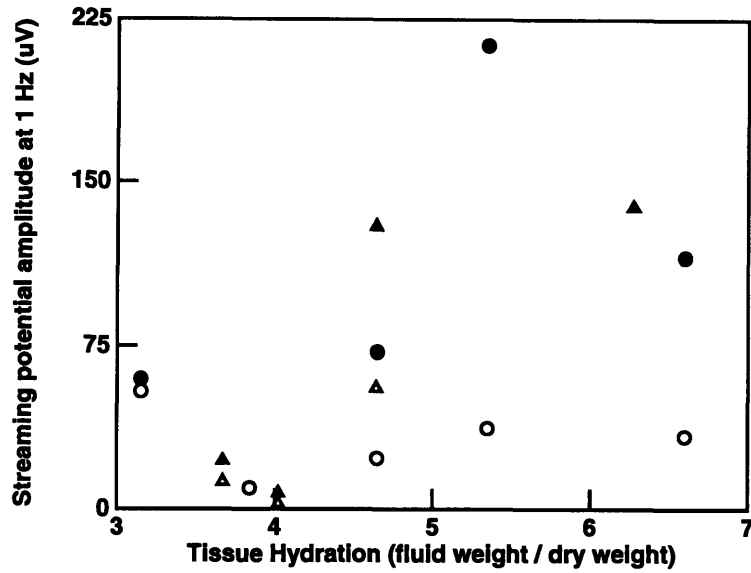
Figure A-11: Scatter plot of $|V_{str}|$ at $1.0 Hz$ versus hydration (ratio of fluid weight to dry weight).
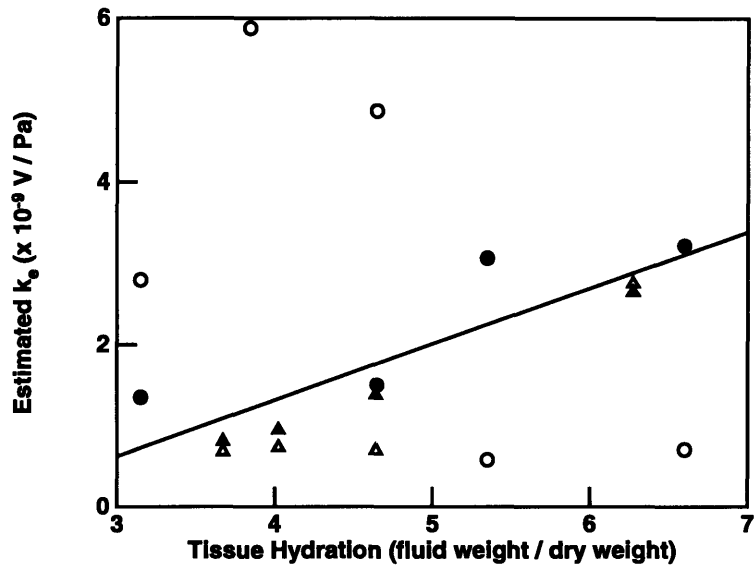
Figure A-12: Scatter plot of k_e versus hydration (ratio of fluid weight to dry weight). Line is fit against deep-oriented data points only, $r^2 = 0.758, p = 0.0049$.
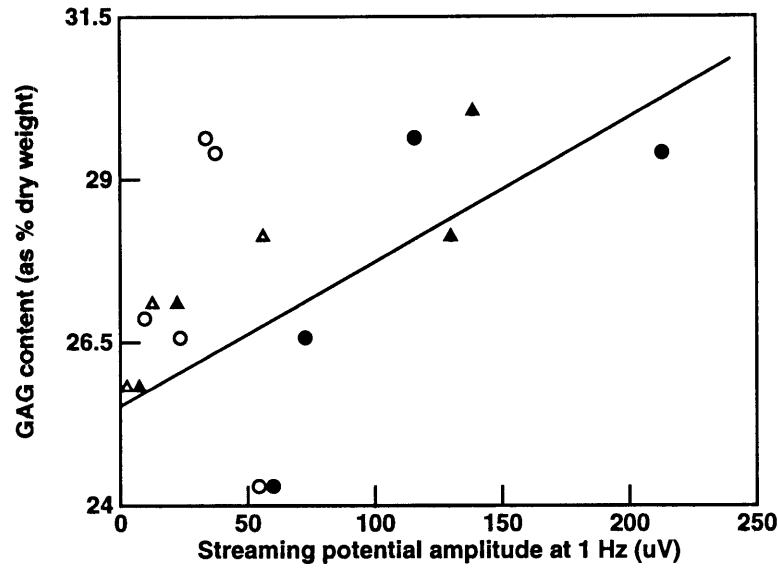
Figure A-13: Scatter plot of [GAG] (as % of dry weight) versus streaming potential amplitude at $1Hz$. Line is fit against deep-oriented data only, $r^2 = 0.543, p = 0.037$.
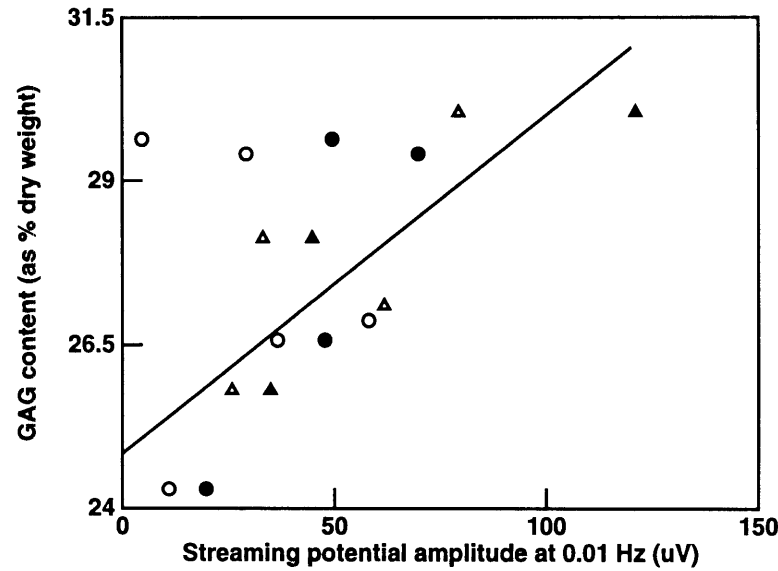

Figure A-14: Scatter plot of [GAG] (as % of dry weight) versus streaming potential amplitude at $0.01Hz$. Line is fit against deep-oriented data only, $r^2 = 0.594, p = 0.043$.
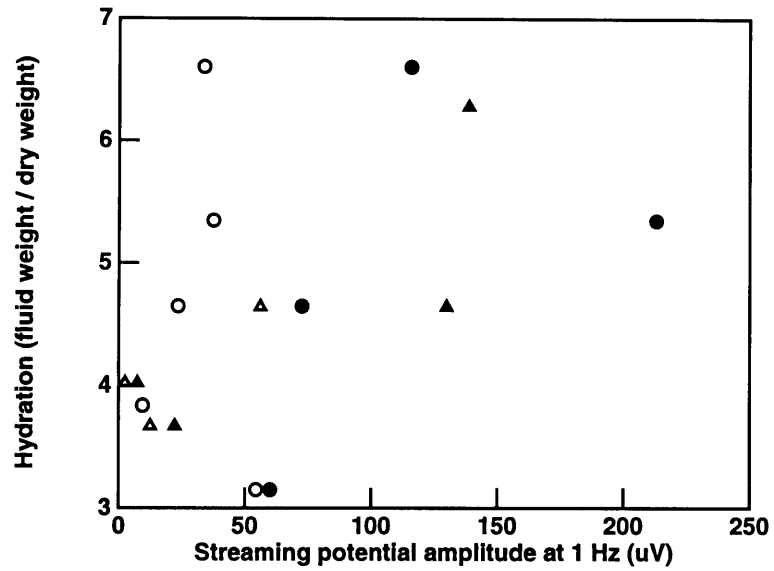
Figure A-15: Scatter plot of tissue hydration H versus streaming potential amplitude at $1Hz$.
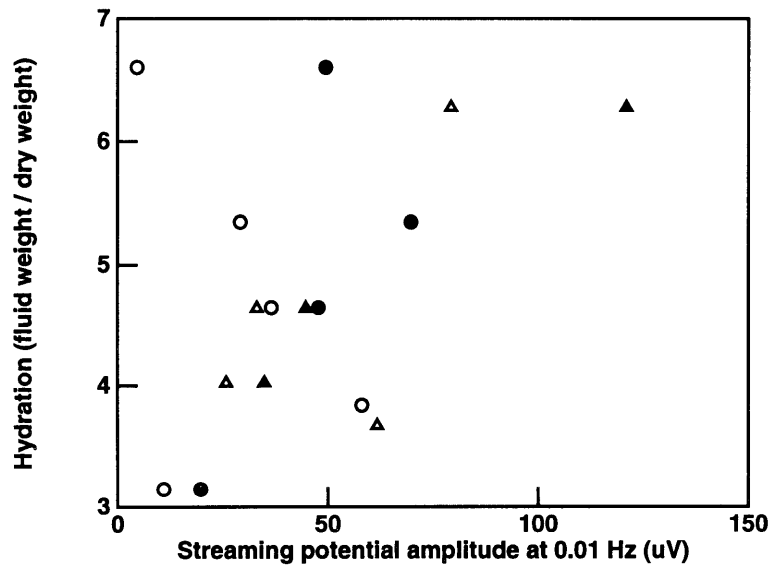

Figure A-16: Scatter plot of tissue hydration H versus streaming potential amplitude at $0.01Hz$.
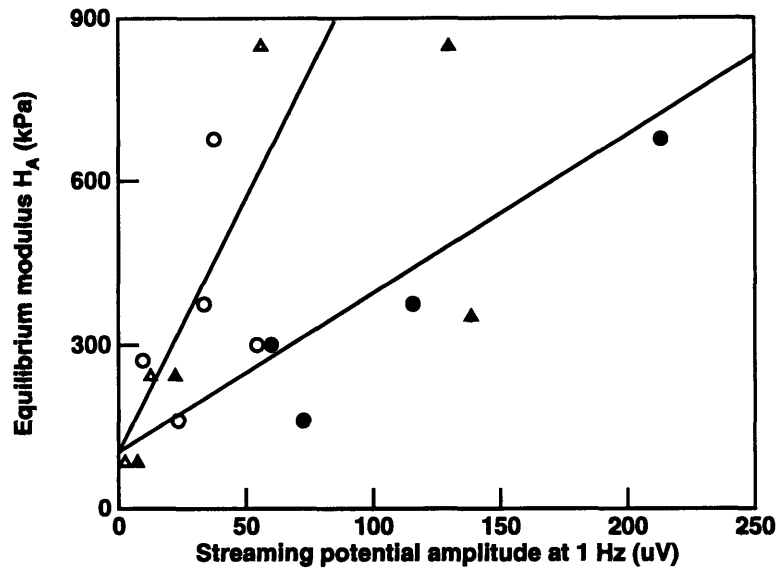
Figure A-17: Scatter plot of H_A versus streaming potential amplitude at $1Hz$. There are two best-fit lines, one against the deep-oriented points only ($r^2 = 0.581, p = 0.028$) and one against the surface-oriented points only ($r^2 = 0.515, p = 0.045$).
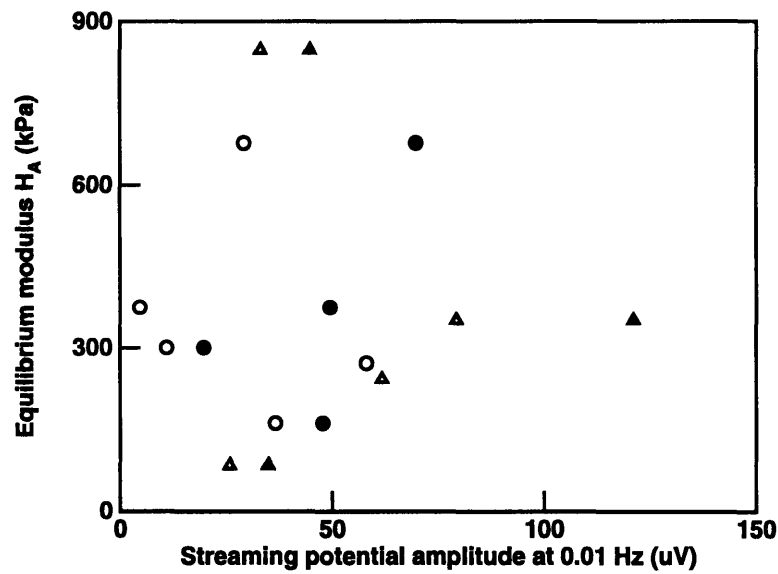

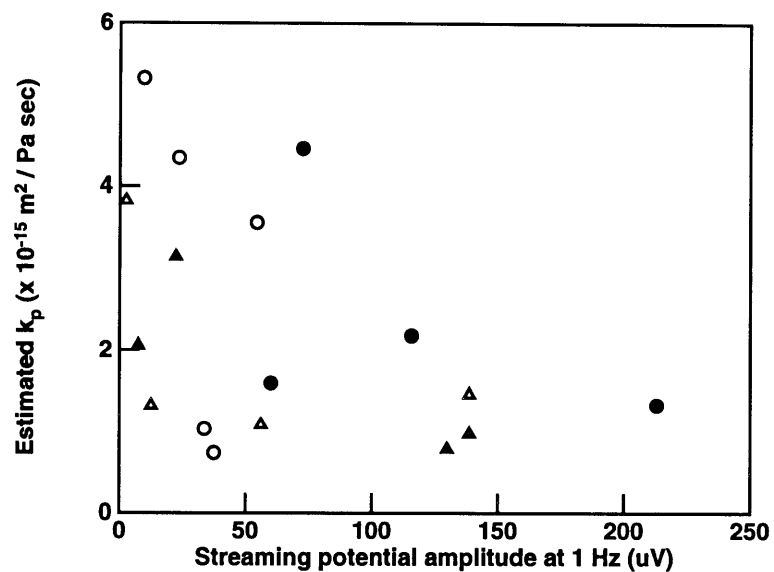Figure A-18: Scatter plot of H_A versus streaming potential amplitude at $0.01Hz$.

Figure A-19: Scatter plot of k_p versus streaming potential amplitude at $1Hz$.
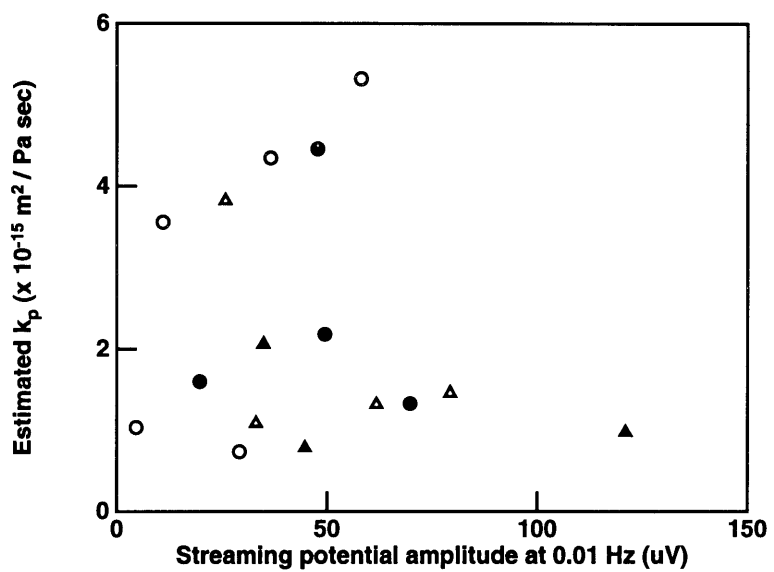

Figure A-20: Scatter plot of H_A versus streaming potential amplitude at $0.01Hz$.

Bibliography

[1] C. G. Armstrong and V. C. Mow. Variations in the intrinsic mechanical properties of human articular cartilage with age, degeneration, and water content. *Journal of Bone and Joint Surgery*, 64-A:88–94, 1982.

[2] K. A. Athanasiou, A. Agarwal, and F. J. Dzida. Comparative study of the intrinsic mechanical properties of the human acetabular and femoral head cartilage. *Journal of Orthopedic Research*, 12:340–349, 1994.

[3] S. I. Berkenblit, E. H. Frank, E. P. Salant, and A. J. Grodzinsky. Nondestructive detection of cartilage degradation using electromechanical surface spectroscopy. *Journal of Biomechanical Engineering*, 116:384–392, 1994.

[4] A. J. Bollet. An essay on the biology of osteoarthritis. *Arthritis and Rheumatism*, 12(2):152–163, 1969.

[5] D. L. Bombard. *A surface probe for* in situ *detection of cartilage degradation via electromechanical spectroscopy*. M.S. thesis, M.I.T., Cambridge, Mass., 1995.

[6] L. J. Bonassar, E. H. Frank, J. C. Murray, C. G. Paguio, V. L. moore, M. W. Lark, J. D. Sandy, J. Wu, D. R. Eyre, and A. J. Grodzinsky. Changes in caritlage composition and physical properties due to stromelysin degradation. *Arthritis and Rheumatism*, 38:173–183, 1995.

[7] J. Buckwalter, E. Hunziker, L. Rosenberg, R. Coutts, M. Adams, and D. Eyre. Articular cartilage: composition and structure. In S. L. Woo and J. A. Buckwalter, editors, *Injury and Repair of the Musculoskeletal Tissues*. American Academy of Orthopaedic Surgeons, Park Ridge, IL, 1987.

[8] R. E. Burgeson and M. E. Nimni. Collagen types. Molecular structure and tissue distribution. *Clinical Orthopaedics and Related Research*, 282:250–272, 1992.

[9] C. E. Carlson, R. W. Mann, and W. H. Harris. A radio telemetry device for monitoring cartilage surface pressures in the human hip. *IEEE Transactions on Biomedical Engineering*, BME-21:257–264, 1984.

[10] S. R. Eisenberg and A. J. Grodzinsky. Swelling of articular cartilage and other connective tissues: electromechanochemical forces. *Journal of Orthopaedic Research*, 3:148–159, 1985.

[11] S. R. Eisenberg and A. J. Grodzinsky. Electrokinetic micromodel of extracellular matrix and other polyelectrolyte networks. *PhysicoChemical Hydrodynamics*, 10:517–539, 1988.

[12] D. R. Eyre, J. Wu, and P. Woods. Cartilage-specific collagens. In K. Kuettner et al., editor, *Articular cartilage and osteoarthritis*. Raven Press, New York, 1992.

[13] R. W. Farndale, D. J. Buttle, and A. J. Barrett. Improved quantitation and discrimination of sulphated glycosaminoglycans by use of dimethylmethylene blue. *Biochimica et Biophysica Acta*, 883:173–177, 1986.

[14] D. T. Felson. Osteoarthritis. *Rheumatic Disease Clinics of North America*, 16(3):499–512, 1990.

[15] E. H. Frank and A. J. Grodzinsky. Cartilage electromechanics—I. Electrokinetic transduction and the effects of electrolyte pH and ionic strength. *Journal of Biomechanics*, 20(6):615–627, 1987.

[16] E. H. Frank and A. J. Grodzinsky. Cartilage electromechanics—II. A continuum model of cartilage electrokinetics. *Journal of Biomchanics*, 20(6):629–639, 1987.

[17] E. H. Frank, A. J. Grodzinsky, T. J. Koob, and D. R. Eyre. Streaming potentials: a sensitive index of enzymatic degradation in articular cartilage. *Journal of Orthopaedic Research*, 5:497–508, 1987.

[18] A. J. Grodzinsky. Electromechanical transduction and transport in the extracellular matrix. *Advances in Microcirculation*, 13:35–46, 1987.

[19] A. J. Grodzinsky and E. H. Frank. Electromechanical and physicochemical regulation of cartilage strength and metabolism. In D. W. L. Hukins, editor, *Connective Tissue Matrix Part 2*. The Macmillan Press Ltd., 1990.

[20] D. Heinegård and Å. Oldberg. Structure and biology of cartilage and bone matrix noncollagenous macromolecules. *The FASEB Journal*, 3:2042–2051, 1989.

[21] D. H. Hoch, A. J. Grodzinsky, T. J. Koob, M. L. Albert, and D. R. Eyre. Early changes in material properties of rabbit articular cartilage after meniscectomy. *Journal of Orthopaedic Research*, 1:4–12, 1983.

[22] W. A. Hodge, K. L. Carlson, R. S. Fijan, R. G. Burgess, P. O. Riley, W. H. Harris, and R. W. Mann. Contact pressures from an instrumented hip endoprosthesis. *Journal of Bone and Joint Surgery*, 71-A:1378–1386, 1989.

[23] D. E. Krebs, C. McGibbon, P. O. Riley, and R. W. Mann. Human acetabular remodeling following femoral implantation. In *Proceedings of the 2nd Annual North American Clinical Gait Conference*, number 3 in Gait and Posture, page 101, Waterloo, CA, 1995.

[24] A. Maroudas. Balance between swelling pressure and collagen tension in normal and degenerate cartilage. *Nature*, 260:808–809, 1976.

[25] A. Maroudas. Physicochemical properties of articular cartilage. In M. A. R. Freeman, editor, *Adult articular cartilage*. Pitman Medical, Kent, England, 1979.

[26] V. C. Mow, M. H. Holmes, and W. M. Lai. Fluid transport and mechanical properties of articular cartilage: a review. *Journal of Biomechanics*, 17:377–394, 1984.

[27] V. C. Mow, S. C. Kuei, W. M. Lai, and C. G. Armstrong. Biphasic creep and stress relaxation of articular cartilage compression: theory and experiments. *Journal of Biomechanical Engineering*, 102:73–84, 1980.

[28] J. G. Peyron. Osteoarthritis. *Clinical Orthopaedics and Related Research*, 213:13–19, 1986.

[29] T. M. Quinn and A. J. Grodzinsky. The longitudinal modulus and hydraulic permeability of poly(methacrylic acid) gels: effects of charge density and solvent content. *Macromolecules*, 26:4332, 1993.

[30] S. Roberts. Mechanical and biochemical properties of human articular cartilage in osteoarthritic femoral heads and in autopsy specimens. *Journal of Bone and Joint Surgery*, 68-B:278–288, 1986.

[31] L. Rosenberg. Structure of cartilage pg. In P. M. C. Burleigh and A. R. Poole, editors, *Dynamics of Connective Tissue Macromolecules*. North-Holland Publishing Company, 1975.

[32] J. R. Sachs and A. J. Grodzinsky. An electromechanically coupled poroelastic medium driven by an applied electric current: surface detection of bulk material properties. *Physicochemical Hydrodynamics*, 11(4):585–614, 1989.

[33] M. Venn and A. Maroudas. Chemical composition and swelling of normal and osteoarthrotic femoral head cartilage: I Chemical composition. *Annals of Rheumatic Disorders*, 36:121–129, 1977.

[34] T. N. Wight, D. K. Heinegård, and V. C. Hascall. Proteoglycans: structure and function. In E. D. Hay, editor, *Cell Biology of Extracellular Matrix*. Plenum Press, New York, 2nd edition, 1991.